Multi-objective optimization of a hybrid carbon capture plant combining a Vacuum Pressure Swing Adsorption (VPSA) process with a Carbon Purification Unit (CPU)

Alexis Costa[a], Arnaud Henrotin[a], Nicolas Heymans[a], Lionel Dubois[b], Diane Thomas[b], Guy De Weireld[a*]

[a] Thermodynamics and Mathematical Physics Unit, University of Mons (UMONS), Place du parc 20, 7000 Mons, Belgium

[b] Chemical and Biochemical Process Engineering Unit, University of Mons (UMONS), Place du parc 20, 7000 Mons, Belgium

* Corresponding author: Email address: guy.deweireld@umons.ac.be

Abstract

The imperative challenge posed by climate change requires urgent actions to counteract the harmful effects of greenhouse gas emissions, particularly CO_2, which contributes to approximately 80% of emissions responsible for global warming. A hybrid system combining Vacuum Pressure Swing Adsorption (VPSA) unit with a Cryogenic Carbon Purification Unit (CPU) is evaluated to enhance recovery and purity of CO_2 captured from flue gas containing CO_2 concentration ranging from 5% to 20%. VPSA preconcentrates the CO_2 and CPU completes the separation and purifies the CO_2. The study uses surrogate models for multi-objective optimization, considering energy consumption, cost, and CO_2 recovery, providing a time-efficient approach for investigating computationally demanding processes. Results from the study indicate that the hybrid system achieves over 90% recovery for flue gas concentration range considered, while ensuring the production of high-purity CO_2 (> 99.99%) suitable for transportation. A trade-off analysis reveals the balance between recovery, electricity consumption, and economic viability. A sensitivity analysis identifies parameters influencing recovery and energy consumption, providing guidance for future optimization efforts. The techno-economic analysis highlights the impact of electricity prices and carbon taxes on total costs, identifying an optimum towards higher recovery values under rising carbon taxes. Furthermore, the research underscores concentration-dependent economic feasibility, emphasizing the attractiveness of concentrations above 10% compared other technologies, which require higher concentrations. For an electricity price of 75 €.MWh^{-1}, the total cost of the CO_2 capture hydride system considering CO_2 emissions with carbon tax of 100 €.t_{CO2}^{-1} for concentrations ranging from 10% to 20% is from 123 to 80 €.t_{CO2}^{-1}, respectively. The analysis of the electricity source shows the importance of a low-carbon emission energy mix for optimal carbon emissions reduction.

Keywords

Carbon capture process, hybrid process, vacuum pressure swing adsorption, carbon purification unit, optimization, techno-economic analysis

1 Introduction

The imperative challenge of climate change needs urgent and impactful actions to limit the harmful effects of greenhouse gas emissions. Among these emissions, carbon dioxide is a major driver of global warming, accounting for approximately 80% of the greenhouse gas emissions responsible for climate change and the main contributor to the greenhouse effect with over 50% compared with other gases [1]. At the COP 21 in Paris, on 12th of December 2015, the Paris Agreement, adopted by 196 Parties, aims to limit global warming to a level well below 2°C, and for the best scenario to 1.5°C, compared to the pre-industrial period [2]. To reach the goal of net-zero emissions, proposed scenarios advocate for a

widespread adoption of renewable energies, steering clear of fossil fuels and prioritizing electrification whenever feasible [1,3].

Nevertheless, a significant percentage of emissions originates from chemical reactions, such as the decarbonation process in cement or lime production (65% of the CO_2 cement plant emissions come from the decarbonation). These CO_2 emissions are unavoidable, regardless of the energy processes employed. Consequently, this underscores the crucial need to develop robust Carbon Capture Utilization and/or Storage (CCUS) systems as one of the solutions to address this issue. Furthermore, the transition to renewable energies will not be instantaneous, necessitating, in transition, the addition of carbon capture systems to functional units to gradually reduce CO_2 emissions. By capturing, utilizing, and storing carbon dioxide emissions, a significant step forward in curbing the impact of industrial processes on the planet's climate can be taken [3].

The CO_2 storage involves transporting it from capture sites to storage locations, whether onshore or offshore. In Europe, offshore storage is currently favored and requires sea-based conveyance. Pipelines or ships are the only two viable options for CO_2 transport. As the distance increases, a tipping point emerges where the cost-effectiveness of shipping surpasses that of pipelines, dependent on specific assumptions [4].

Ensuring safe and efficient maritime transport of CO_2 requires stringent specifications. For instance, maintaining O_2 levels below 10 ppm and H_2O content below 30 ppm becomes imperative to mitigate the risks of corrosion [5]. These conditions remain relatively consistent for pipeline transport, with values that may vary based on the source, akin to the variation in water vapor levels (40 to 650 ppm) [5,6]. Moreover, when catalysts are involved in CO_2 conversion field, the utilization aspect necessitates specific high CO_2 purity to prevent catalyst deactivation or the formation of undesirable by-products [7]. This aspect assumes great significance when analyzing the entire CCUS process chain, aiding in the determination of the required purity level for CO_2. Comprehensive consideration of these factors enhances the efficacy and sustainability of carbon capture initiatives.

Various adaptations of existing industrial processes have been developed to incorporate carbon capture technologies, including pre-combustion, oxy-combustion, and post-combustion techniques [8].

Post-combustion technologies focus on extracting CO_2 from a flue gas at the end of the process chain, necessitating minimal modifications to the industrial plant. However, a disadvantage is that the flue gas is more diluted, which results in increased energy consumption associated with the capture processes. Typical CO_2 contents of flue gases coming from: gas power plant: ±5%, waste burner: ±10%, coal power plant: ±15% and lime or cement plant: ±20% [9]. Each approach offers unique advantages and challenges, and selecting the most suitable method depends on the specific characteristics of the industrial process and the desired level of CO_2 capture [10].

Various technologies are available for carbon capture, such as absorption, adsorption, membrane technologies and cryogenics [11]. Chemical or physical absorption involves using a solvent with a high affinity for CO_2 to capture it in an absorber, which can then be regenerated in a stripper through the application of thermal energy [12]. Amines-based solvents currently serve as the benchmark due to their maximum Technology Readiness Level (TRL) thanks its development in the 1930s to extract CO_2 from natural gas [13]. The generated CO_2 is relatively pure with classic target of 98 mol% CO_2, requiring only a drying unit for transportation. However, they come with several drawbacks, such as thermal or oxidative degradation into toxic chemicals which can have health impacts or such as volatility, which can have significant environmental and health impacts. Another concern is the thermal consumption required for the solvent regeneration, necessitating steam generation, which introduces new emissions if no fatal excess heat is available at the industrial site [14].

Adsorption uses solid materials like active carbon, zeolite, Metal Organic Frameworks (MOFs) with a strong affinity for CO_2, allowing it to be retained within the material's pores during the adsorption phase

and released when a Pressure Swing Adsorption (PSA), Vacuum Swing Adsorption (VSA) or Temperature Swing Adsorption (TSA) differential is applied during the regeneration phase of the adsorbent [15]. There is an optimum trade-off between two performance indicators, namely CO_2 purity and recovery, necessitating to define a compromise between them or requiring two units to achieve both performances. In addition, this process can be sensitive to water reducing the adsorption performances depending on the adsorbent used.

Membrane technologies, primarily polymer-based, enable CO_2 separation from other molecules by applying pressure differentials across the membrane, allowing molecules to permeate [16]. However, achieving recovery higher than 90% with 95-99 mol% CO_2 purity requires also duplicating units, leading to increased capital expenditure (CAPEX) and site footprint.

Cryogenics involves manipulating temperature conditions to liquefy or sublimate flue gas, separating CO_2 from other processes. Carbon Purification Unit (CPU) works well for high concentrated flue gas from oxy-combustion by partially liquefying the stream [17]. Cryogenic Carbon Capture (CCC) can treat post-combustion flue gas by sublimate the CO_2 [18]. Cryogenics offers highly pure CO_2 at the process output, yet energy consumption and operational expenditure (OPEX) are significant for flue gas in post-combustion conditions due to the low CO_2 concentration in the inlet flue gas [19].

All capture techniques present efficiency, scalability, and cost-effectiveness advantages and challenges. Ongoing research aims to optimize these methods for broad application in industries such as power generation, cement production, and natural gas processing. Considering the necessary specifications for gas transport or post-capture utilization, it is crucial to explore wider boundaries in capture unit design to take into account for final CO_2 purification requirements. Based on these considerations, the present study's objective is to investigate a hybrid system capable of producing CO_2 reaching required CO_2 specification for transportation or utilization with catalyst while minimizing energy consumption.

Numerous investigations have explored hybrid post-combustion systems, as described by Song et al. [20], employing processes commonly organized in a sequential manner. For instance, by combining membrane-absorption [21], membrane-adsorption [22], adsorption-membrane [22], cold membrane integrated into a cryogenic unit [23–26], or adsorption-cryogenics [27] approaches. In the present work, a hybrid system that combines a Vacuum Pressure Swing Adsorption (VPSA) process with a high purity cryogenic carbon purification unit is considered, following the concept outlined by Rodrigues et al. [28,29]. The combination of these two technologies makes it possible to mix high CO_2-recoveries of VPSAs and high CO_2-purities of CPUs, resulting in an optimized capture process that combines both qualities.

Adsorption has already demonstrated its effectiveness in gas treatment, whether in refineries to purify hydrogen produced by Steam Methane Reforming (SMR), or in natural gas extraction to purify methane from carbon dioxide. PSA allows to perform rapid cycle compared to TSA which limits the investment costs. The main drawback of PSA process is the electrical energy required. Therefore, the optimization of energy consumption is an essential point to design an efficient separation unit [30,31]. In the literature, numerous PSA processes have been developed for CO_2 capture. Since the flue gas is already at atmospheric pressure, VPSA processes are preferred due to the better selectivity at low adsorbent loading [30,32]. Several adsorbent and cycle configurations have been studied for CO_2 capture with VPSA process. Among the numerous materials available (active carbon, zeolite, MOF, etc.), zeolite 13X is one of the most interesting materials, exhibiting high CO_2 adsorption capacity and selectivity at low and moderate partial pressure of CO_2 (0.05-0.5 bar) and ambient temperature. For a 15/85% CO_2/N_2 mixture at 1 bar and 25 °C, the CO_2 adsorption capacity is around 2.5 to 3.5 $mmol.g^{-1}$ with a selectivity between 150 and 850 [33–35] and for 5% CO_2 at 1 bar et 25°C, the selectivity remains higher than 100 with a capacity higher than 1 $mmol.g^{-1}$ [34]. Nevertheless, zeolite 13X is sensitive to contaminants such as NO_x or SO_x reducing the CO_2 adsorption capacity of the material. Water is also a concern for this material since zeolite is a hydrophilic material, making the adsorption of water preferential instead of

CO_2. Presence of water vapor in flue gas leads to a drastic reduction of the CO_2 adsorption capacity of the zeolite, and a reduction of performance in VPSA cycle. Therefore, a pretreatment line is required to remove contaminants and water before the VPSA unit [32,34,36,37].

VPSA processes can be operated with different cycle configurations depending on the number of adsorption beds used, and the sequence of steps performed. Skarstrom cycle is the first (V)PSA cycle developed and consists of an adsorption, blowdown, purge, and pressurization step [38]. A pressure equalization step can be used between adsorption and blowdown to improve the performance of the cycle [30,31,38]. This cycle was already tested for CO_2 capture with activated carbon on a laboratory pilot allowing to reach a CO_2 recovery of 96.16% and a CO_2 purity of 63.04% for a flue gas containing 15% of CO_2. This result was obtained with a vacuum pressure of 0.1 bar and an adsorption pressure of 3.25 bar [39]. Jiang et al. [40] studied this cycle through simulation works with zeolite 13X showing CO_2 recovery higher than 95% and purity higher than 50% for a desorption pressure of 0.06 bar and an adsorption pressure of 1.5 bar. Skarstrom cycle with pressure equalization was also simulated by Liu et al. [41] obtaining 93% of CO_2 recovery and 58% of purity for 15/85 CO_2/N_2 mixture, a blowdown pressure of 0.15 bar and adsorption pressure of 1.5 bar. Other 2-column configurations have been developed to capture CO_2 in post-combustion. Zeolite 13X was tested by simulation and experimentally on a 4-step cycle including adsorption, co-current blowdown, counter-current blowdown, and pressurization from the gas coming from the adsorption step. Results obtained from this cycle give a high CO_2 recovery (86.4%) and purity (95.9%) with a single unit [42–44]. Nevertheless, the vacuum pressure used is very low (0.011 bar), which significantly increases the energy consumption of the vacuum pump and leads to unrealistic conditions for an industrial process. Moreover, the cycle includes idle step where the flue gas is not treated requiring more units or a gas tank to process the flue gas in a continuous way. More adsorption beds can be used to increase the performance of a VPSA unit. 3-bed 5-step cycle including rinse step was studied with 13X by simulation in order to reach higher CO_2 purity than Skarstrom cycle with the same pressure level (adsorption = 1.5 bar and blowdown 0.1 bar). The unit is able to reach almost 99% of CO_2 recovery with a purity of 65% [45]. 3-bed with 6-step, 9-step and 12-step were studied to reach purity higher than 90% in a single unit. This purity can be achieved by the mean of low vacuum pressure (0.03 bar), and recovery between 60 and 70% [46,47]. Even if the 3-bed configuration allows to increase the performance of the VPSA unit, the amount of adsorbent required by kg of CO_2 captured and the capital investment are generally higher than 2-bed configuration.

Several studies [19,48–55] have addressed their interest on CPU technology, examining its adaptability to different oxy-combustion flue gas compositions with CO_2 concentrations ranging from 75 to 95 mol% (dry basis). Remarkably, CPU can achieve CO_2 recovery rates as high as 90%, although the potential exists for even higher recoveries, depending on the initial CO_2 concentration at the system inlet. Achieving the desired purity levels depends largely on the inclusion of unitary operations in the CPU process, such as a distillation column or a desorber.

Two main types of CPUs: medium purity CPU and high purity CPU. The medium purity CPU, often equipped with 1 or 2 flash separators, can deliver CO_2 with a purity of 95 mol%. The high purity CPU, on the other hand, is equipped with a column system that allows it to consistently exceed the coveted 99 mol% purity level and even achieve food-grade CO_2 quality [56]. In terms of energy consumption, it should be noted that the high purity CPU typically consumes 10 to 15% more electrical energy compared to its medium purity counterpart [48,52,55]. This discrepancy in energy consumption results from the more complex separation processes required to achieve high CO_2 purity.

Consistent with the general principles of carbon capture, it's also important to recognize that the energy required for CO_2 capture decreases as the initial CO_2 concentration in the flue gases increases. Values range from about 164 $kWh.t_{CO2}^{-1}$ captured for flue gases containing 75 mol% CO_2 [51] to a more efficient 112 $kWh.t_{CO2}^{-1}$ for flue gases containing 94 mol% CO_2 [52]. This progressive reduction in energy demand highlights the potential energy saving benefits of CPU systems, particularly when used in

environments with higher CO_2 concentrations, and contributes to more sustainable and economically viable carbon capture solutions.

In this work, a 2-bed VPSA was chosen to generate pre-concentrated CO_2 flux at a minimum of 50 mol%. This value corresponds to the entry level at which the CPU becomes energetically interesting. For the CPU, a purity of 99.999 mol% is targeted in order to avoid any trace of undesirable compounds for CO_2 transport or conversion operations. Aspen Plus® and Aspen Adsorption® V14 were used to model cryogenic and VPSA units, respectively. Surrogate models, which convert process simulations into mathematical representations, are employed to facilitate the optimization of the process, aiming to analyze diverse performance indicators including energy consumption, cost, and CO_2 recovery. These models play a pivotal role in identifying the most advantageous operational parameters for the processes. The application of such tools in a hybrid setup stands as a noteworthy innovation, offering substantial time savings in investigating simulated processes that entail computationally demanding calculations. Optimizing two processes simultaneously provides an advantage over optimizing each process individually to ensure finding the optimum point. This work provides a detailed energetic and economic study of this innovative process, and a methodology for performing multi-objective optimization of a complex, fully integrated process.

2 Details and design of the process

2.1 Process configuration

The studied process is a hybrid combination of a vacuum pressure swing adsorption and a carbon purification unit used to capture the CO_2 from flue gases with a CO_2 concentration between 5-20 mol% and a flow rate of 70,000 $Nm^3.h^{-1}$ corresponding to around 1000 $t.d^{-1}$ of clicker production (see Figure 1). To prevent deterioration of the adsorption performance and ice formation in the CPU, the flue gas is considered as dehydrated upstream of the process. To achieve the dehydration required for the VPSA and the CPU, TSA with silica gel or alumina must be used to dry flue gas before the CO_2 capture unit [57,58]. It is also necessary to consider potential treatments on a larger scale to remove pollutants that could degrade the material, such as dusts, NOx, SOx, Hg, etc. In this study, a preliminary assumption is to focus solely on nitrogen and carbon dioxide. The VPSA is used to concentrate CO_2 from the flue gas at least 50 mol% CO_2 before remove the rest of the impurities in the CPU. The CPU purifies the CO_2 through the liquefaction of the flue gas, allowing to separate liquid CO_2 from the incondensable gases. These are sent back to the VPSA to recover the CO_2 that has not liquefied in the CPU. Finally, a minimum purity of 99.999 mol% is obtained at the output of the CPU. The total process CO_2 recovery depends on the impact of CPU recycle on the VPSA. Traditionally, the target for capture processes is to achieve 90% recovery even if in recent papers, this target increases to reach a value of 95% or more. Nevertheless, this value could be higher while remaining economically viable. That's why in this study, recovery will be an optimization objective.

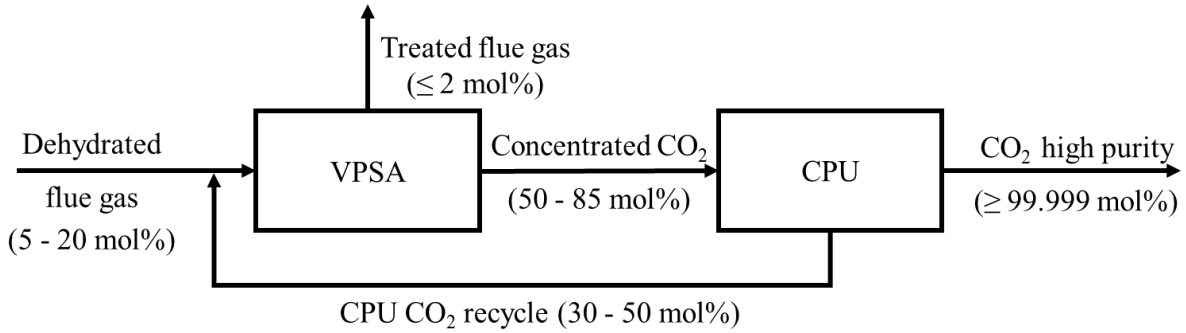

Figure 1: Hybrid VPSA-CPU CO_2 capture process.

The objective of this work is to minimize the electrical consumption of the CO_2 capture process by globally optimizing the hybrid process, VPSA and CPU. Each process can be optimized for a specific CO_2 recovery and purity by minimizing the electrical consumption that is associated with a large part of the capture process cost. When the two processes are combined, the CO_2 recovery is fixed at the VPSA level, and the final CO_2 purity is determined with the CPU performance. This means that there is flexibility in the purity of the CO_2 at the VPSA output, which will have an impact on the electrical consumption. At fixed recovery, the more concentrated the CO_2 is, the higher the electrical consumption of the VPSA will be, but the lower the electrical consumption of the CPU will be. It is important to retrieve the right balance between the CO_2 purity and the electrical consumption of the VPSA and CPU in order to minimize the overall electrical consumption of the entire CO_2 capture process. Moreover, the recycled flux to the VPSA can modify the performances of the adsorption unit leading to different results in terms of purity, recovery, and energy consumption.

2.1.1 VPSA modelling

The first part of the process is a 2-bed VPSA unit performing the Skarstrom cycle with pressure equalization step [31]. Sequence of steps for one bed, in addition with the pressure profile is represented on Figure 2. The first step of the cycle is the adsorption where the flue gas is sent to the column to adsorb mainly the CO_2 and to obtain a nitrogen-rich gas at the outlet of the column. The column is then connected to the second column which is at lower pressure to equalize the pressure and save mechanical work of compression and vacuum. The pressure is further reduced in the blowdown step to desorb the CO_2 in the column and retrieve it. A part of the nitrogen-rich stream of the column in adsorption step is used during the purge step to flush the CO_2 from the second column and increase the amount of CO_2 retrieved. Finally, the two columns are connected for the equalization of pressure, followed by a pressurization from the flue gas until the adsorption pressure is reached. In this cycle, the time of the blowdown step and the purge step must be equal to time of the adsorption step and pressurization step to keep the synchronization between the two beds.

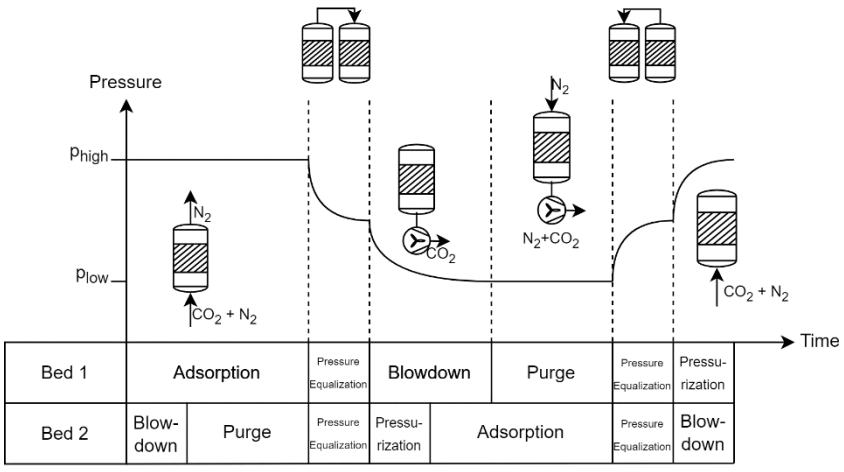

Figure 2: Sequence of steps and pressure profile for the cycle used in the VPSA unit.

Zeolite 13X (UOP MOLSIV^{TM}) was chosen for its good CO_2/N_2 separation performance in dry conditions (CO_2 adsorption capacity, selectivity, etc.), the results already proven in simulation and pilot scale VPSA process for post-combustion CO_2 capture, and its commercial availability [43,44,46,47,59–61]. Adsorption isotherms, kinetics, and other parameters relative to zeolite 13X were obtained from literature data [62,63]. In these works, adsorption isotherms for CO_2 and N_2 are modelled with a dual-site Langmuir model with temperature dependency given by equations (S7) to (S9) in Supporting Information. Parameters of the adsorption isotherm model are given in Table 1 and are thermodynamically consistent which ensure a better representation of the co-adsorption as demonstrated by Farmahini et al. [62]. In addition, the affinity parameters for N_2 are equals ($b_0 = d_0$ and $\Delta H_1 = \Delta H_2$)

Other parameters relative to the adsorbent are given in Table 2. The adsorbent is assumed to have a spherical shape with a diameter of 3 mm. The packing density was derived from the crystal density of zeolite 13X (1403 $kg.m^{-3}$) [62] and the inter- and intraparticle void fraction [63–65]. Tortuosity of the adsorbent is obtained from Hu et al. [63].

Table 1: Adsorption isotherm parameters used for zeolite 13X (from [66]*).*

Parameter	CO_2	N_2
q_{s1} [$mmol.g^{-1}$]	1.44	1.44
b_0 [bar^{-1}]	3.59×10^{-5}	2.89×10^{-7}
ΔH_1 [$J.mol^{-1}$]	40.014×10^3	30.67×10^3
q_{s2} [$mmol.g^{-1}$]	3.47	3.47
d_0 [bar^{-1}]	8.27×10^{-5}	2.89×10^{-7}
ΔH_2 [$J.mol^{-1}$]	40.491×10^3	30.67×10^3

Table 2: Geometric parameters of Zeolite 13X (from [67]*).*

Parameter	Value
Packing density [$kg.m^{-3}$]	645.24
Inter-particle void fraction [-]	0.37
Intra-particle void fraction [-]	0.27
Pellet diameter [mm]	3
Tortuosity [-]	2.6

To process the 70,000 Nm^3/h of flue gas, five VPSA units are working in parallel to treat initially 14,000 Nm^3/h of flue gas. The volume of the bed used is equal to 80 m^3 with an inner diameter of 3.24 m and length of 9.71 m filled with spherical beads of 3 mm diameter. The dimensions of the pilot were chosen to avoid the fluidization of the bed, and decrease the pressure drop of the units. The complete sizing procedure based on pressure drop and minimum fluidization velocity is described in Supporting Information.

The VPSA unit was modelled in Aspen Adsorption® V14 software using a 1D discretization in 30 nodes of the bed using the Van Leer scheme and the "unibed" approach which simulates a single bed to save simulation time [68]. Flowsheet used in the simulation software is represented in Figure S3 in Supporting Information. Plug flow is used for mass balance including axial dispersion, convective flow, accumulation in gas phase and accumulation in adsorbed phase represented by equation (S4) [30]. Axial dispersion coefficient is obtained with the correlation from Langer et al. [69] (equation (S11)). Linear driving force [70] given by equation (S14) is used to represent the adsorption kinetics. Macropore diffusion model is used to compute the kinetic coefficient (equation S15) with the parameters from

Table 2 [63]. Ergun equation is used for the momentum balance of the bed as represented in equation (S16). The bed is considered as non-isothermal with energy balance for the gas (equation (S17)), solid (S18), and wall of the bed (S19). The energy balance of the gas is composed of thermal conduction, convection, accumulation, heat generation from adsorption, gas-solid heat transfer, and gas-wall heat transfer. For the solid phase, only accumulation of heat in the solid is considered, neglecting the heat of the adsorbed phase. For the wall of the bed, accumulation, axial conduction, conduction across the wall and gas-wall heat transfer for the inside and outside of the column are considered [30,71]. The following correlations were implemented in Aspen Adsorption® V14 for the computation of the heat transfer coefficient:

- Heat transfer coefficient between solid and gas: correlation of Whitaker [48][72] given by equation (S20) which is valid for $20 < Re < 10{,}000$ and $0.34 < \varepsilon_b < 0.78$.
- Heat transfer coefficient between gas and wall: Correlation of Beek [72,73] (equation (S21)) which is valid for $40 < Re < 2000$.

- Heat transfer coefficient between wall and ambient: general heat transfer correlations for natural convection and radiation [72,74,75] represented by equation (S22) to (S25).

All the parameters used for the VPSA simulation are listed in Table S1 of Supporting Information. In addition, the gas properties (density, viscosity, heat capacity, heat conductivity) are determined with Aspen Properties V14 software using the following models :

- Redlich-Kwong-Soave equation of state for gas density [76].
- Chapman-Enskog-Brokaw with Wilke mixing rule for gas viscosity [77,78].
- Wassiljewa-Mason-Saxena model for heat conductivity [79].
- Polynomial model with data from [80] for gas heat capacity.

.

VPSA unit is evaluated with the purity and recovery of CO_2 obtained in addition to the electrical consumption. Purity is obtained by summing the amount of CO_2 obtained in the product section during one cycle, divided by the total amount obtained in this same section (equation (1)). VPSA recovery is the fraction of CO_2 retrieved at the outlet of the VPSA unit compared to the CO_2 in the flue gas. It is computed by the amount of CO_2 obtained in the product section divided by the amount of CO_2 in the feed gas (equation (2)) [31][33].

$$Purity_{VPSA} = \frac{\sum_{cycle} \dot{n}_{product} y_{CO_2\ product}}{\sum_{cycle} \dot{n}_{product}} \quad (1)$$

$$Recovery_{VPSA} = \frac{\sum_{cycle} \dot{n}_{product} y_{CO_2\ product}}{\sum_{cycle} \dot{n}_{feed} y_{CO_2\ feed}} \quad (2)$$

where $\sum_{cycle}$ is the sum of the various time intervals in the cycle, $\dot{n}$ is the molar flow rate (mol.s^{-1}) and y_{CO_2} the CO_2 molar fraction in the feed or in the product.

Cycles were performed until cyclic steady state was reached. During the pressure equalization steps, the flue gas is not treated by the VPSA unit. To take this into account, it is assumed that a buffer gas storage allows for the temporary regulation of the gas flow. VPSA purity and recovery are evaluated at the end of every cycle and compared with the values obtained during the previous cycle. The simulation is stopped when the difference is lower than 0.1% for both indicators. Seven parameters have been studied for the VPSA unit. The parameter bounds were chosen to cover a relatively wide range, considering the subsequent integration with the CPU. Among parameters, there are adsorption time [60 – 2000 s], purge time [10 – 1990 s], equalization time [10 – 50 s]. For these three parameters, a minimum time of 10 seconds for each step, leading to a minimum adsorption time of 60 seconds. The maximum adsorption time was obtained by increasing the upper bound in order to ensure that the optimization results do not stick to the upper bound. The maximum purge time was adapted from the adsorption time minus 10 seconds for blowdown. The maximum equalization time was set to 50 seconds since this step should be as fast as possible. In addition, adsorption pressure [1.01325 – 3 bar], blowdown pressure [0.01 – 0.5 bar], feed flow rate [14,000 – 25,000 Nm³.h^{-1}] (extra flow rate above 14,000 Nm³.h^{-1} is the recycle gas from the CPU and the factor [*(adsorption time + equalization time)/adsorption time*] considering the zero flow rate during the equalization step), purge flow rate [100 – 20,000 Nm³.h^{-1}] and feed CO_2 concentration [5 – 27%] (the recycle gas from VPSA is concentrated between 30 and 50 mol% CO_2 that increases the concentration of the flue gas at the VPSA inlet) are also studied. For feed flow rate and CO_2 concentration, the upper bounds were obtained by preliminary simulations of the CPU unit giving the flow rate and CO_2 concentration of the recycled flow from the CPU to the VPSA unit. The purge time was always chosen to be lower than the adsorption time, and the difference between adsorption time and purge time (which is equal to blowdown time) must be at least 10 s. For pressurization, this step was included in the adsorption step by sealing the outlet of the adsorption bed at the beginning of

the adsorption step, increasing the pressure with the feed gas. When the pressure inside the bed reaches the desired adsorption pressure, the valve at the outlet of the bed is automatically opened.

2.1.2 CPU modelling

The second part of the process is the CPU. This unit is inspirited by the Air Liquide Callide project [81,82] and based on the study performed by Costa *et al.* [83]. A schematic of this process is proposed on Figure 3. Six fundamental steps are present: (1) flue gas compression, (2) flue gas cooling, (3) CO_2 vapor-liquid separation, (4) CO_2 purification, (5) cold generation and (6) CO_2 compression. This unit purifies the CO_2 pre-concentrated by the 5 VPSA units. The minimum concentration at the inlet of the CPU is 50 mol% CO_2 to stay energetically interesting.

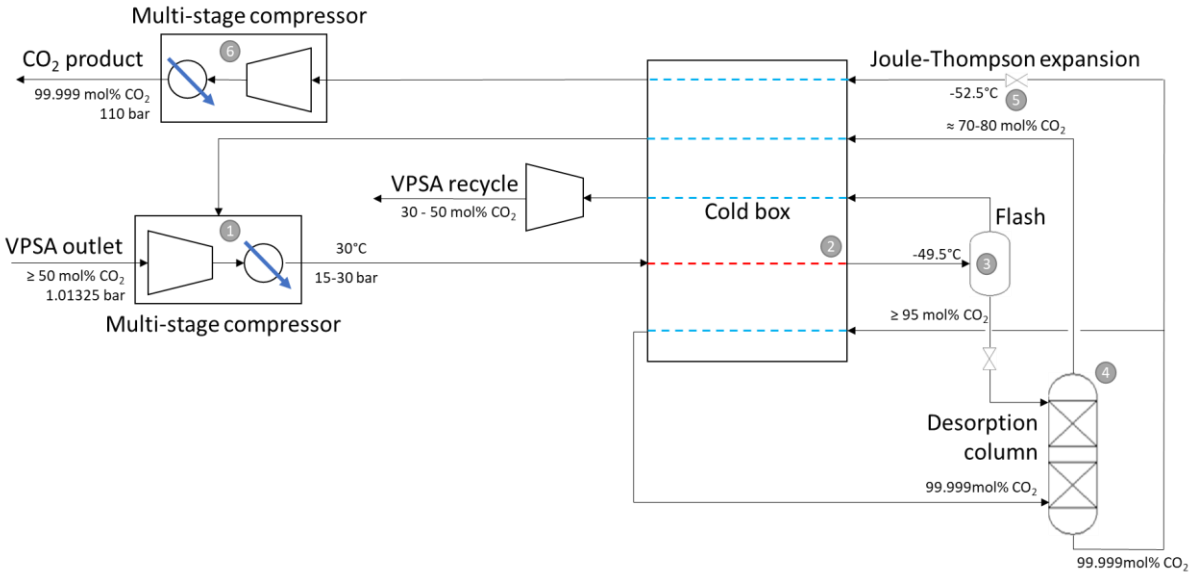

Figure 3: Schematic plan of the CPU.

The cryogenic unit plays a crucial role in purifying carbon dioxide (CO_2) and removes incondensable gases. This separation process is achieved by utilizing the unique properties of cryogenics, particularly the liquefaction of CO_2. To ensure efficient separation without the formation of dry ice (solid CO_2), a carefully controlled temperature limit of -54 °C is established. This temperature is deliberately kept just above the triple point of -56.6 °C at which CO_2 transitions between its solid, liquid, and gaseous phases.

The concentrated CO_2 from the 5 VPSA units passes through a multi-stage compression system that includes intercooling with water (1). To achieve the flue gas liquefaction, multi-stream brazed aluminum heat exchanger (BAHX) is employed (2). The effectiveness of this technology has been successfully demonstrated in previous projects such as the Callide project [81].

After liquefaction step, the liquid CO_2 is separated from non-condensable gases by using a flash separator (3). This separation step ensures that liquid CO_2 (> 95 mol%) enters the process. To avoid losing the coldness from these gases, it can be efficiently recovered and utilized through BAHX. These gases are then expanded to generate energy before being returned to the VPSA processes, optimizing the overall efficiency of the plant.

The liquid CO_2 is then fed into the desorption column (4). In this column, the impurities are effectively stripped by pure CO_2 vapor. This desorption process is fundamental to achieving a high CO_2 purity of 99.999 mol%.

To further increase the efficiency of the plant, a fraction of the product liquid CO_2 is heated to provide pure CO_2 vapor to the column, while the remaining fraction is subjected to Joule-Thompson expansion (5). Then, the product CO_2 is compressed to reach the required supercritical pressure for injection into

the pipeline distribution network, typically 110 bar (6). The expansion process generates the refrigeration required for liquefaction, contributing to the overall energy efficiency of the system.

Figure 4 is the modelling in Aspen Plus® V14 software. The Peng-Robinson equation of state [84] was chosen to determine the thermodynamic properties of the fluid mixture. The binary interaction parameter k_{ij} for CO_2-N_2 is -0.017 [85]. The first multi-stage compressor has 4 stages, resulting from an optimization between CAPEX and OPEX using the cost calculation defined in the 2.3 section. Pressure ratio is kept between 2 and 5 to limit the compressed gases temperature to a maximum of 200 °C [86]. Regarding the process cooling, two Joule-Thompson expansions are used to reduce the electrical consumption thanks to the fact that a fraction of the liquid flow rate expand to a higher pressure in the valve V2 than in the valve V3 which must generate a stream at -52.45°C. The produced CO_2 is conditioned to a supercritical state to be transported at 110 bar. Thus, the CO_2 is compressed up to 72 bar with 4 stages of compression in order to be liquefied under the critical point before being pumped up to 110 bar. This process part consumes less electricity (7% for water cooling temperature of 20 °C) than a 5 stages compression as presented in [87]. Table 3 presents the various hypotheses defined for CPU modelling.

Table 3: Assumption for the CPU modelling.

Assumptions	**Value**
Minimum temperature	-54 °C
Water cooling temperature	20 °C to 25 °C
BAHX pressure drop	0.45 bar
Heat exchanger pressure drop	0.1 bar
Desorption column packing	Mellapak 250Y

In this process, seven parameters are under scrutiny to optimize the efficiency of the integrated process. The CO_2 concentration [50 – 85%] and gas flow rate [1,000 – 40,000 $Nm^3.h^{-1}$] at the CPU inlet span a broad range, accommodating various potential scenarios from the VPSA. Adjusting the pressure of the cold box [15 – 30 bar] (compressor C4) plays a crucial role in modifying the liquid-vapor equilibrium at the FL1 flash. This equilibrium significantly influences both the flow rate and the CO_2 concentration of the recycled stream directed towards the VPSA.

The desorption column pressure [9 - 17 bar] and the mass fraction towards the column of splitter S1 [0.05 – 0.20] are fitted to achieve the desired CO_2 purity. Recycling the vapor emanating from the column before compressor C4 is also a crucial step. To optimize the compression stages, the outlet pressure of compressor C3 is strategically set in relation to the column pressure, considering pressure losses. These parameters collectively influence the amount of vapor recirculated with the flue gas and the pressure set for the initial Joule-Thompson expansion V3, important for process cooling.

Finally, the pressure of the second Joule-Thompson expansion [7 – 14 bar] and the mass fraction towards the first Joule-Thompson expansion of splitter S1 [0.05 – 0.75] are systematically varied to fine-tune the amount of refrigeration necessary for the efficient operation of the entire process.

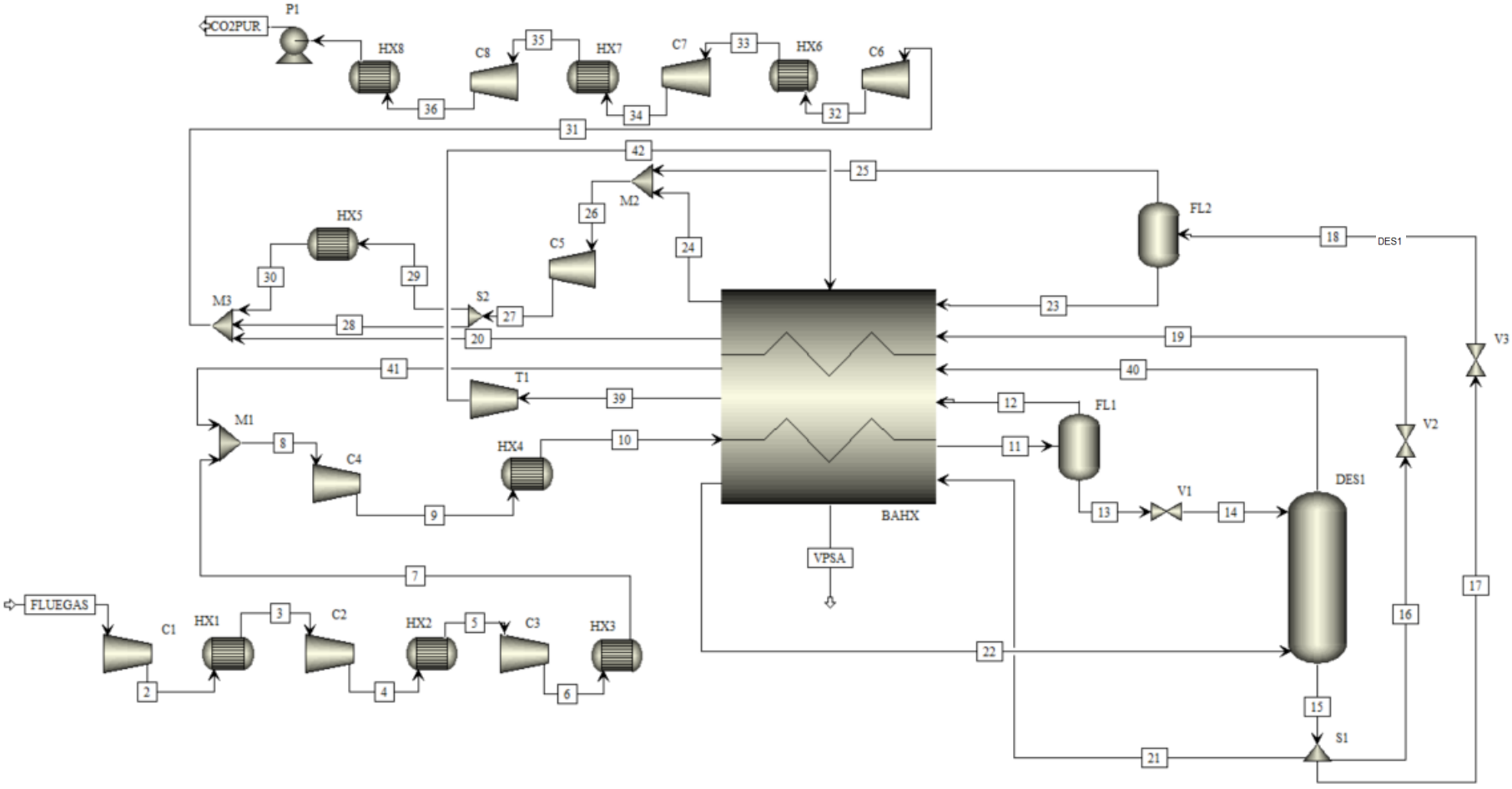

Figure 4: Aspen Plus® V14 flowsheet of the CPU.

2.2 Energy balance

Electrical consumption of each VPSA unit is due to compressor and vacuum pump, and for CPU from compressors and liquid pumps including an energy recuperation from the turbines. The electrical consumption for compressors and vacuum pumps is evaluated with equation (3) where p_{low} is the inlet pressure, and p_{high} is the outlet pressure. For vacuum pump, p_{high} is the atmospheric pressure. Isentropic efficiency (η_{iso-s}) is set to 85% for compressors. For vacuum pump, isentropic efficiency varies in function of the pressure and is calculated following equation regressed in the Subraveti *et al.* study [88]. The energy retrieved from the turbines of the CPU is evaluated with a similar equation (4) where p_{low} is the outlet of the turbine and p_{high} the inlet. The isentropic efficiency of the turbine is equal to 90%. For pumps, equation (5) is used with an efficiency of 72.5 %. The total electrical consumption of the hybrid unit by mass of CO_2 captured is given by equation (6) by summing the electrical consumption, and by dividing by the sum of CO_2 obtained.

$$\dot{W}_{compressor\ \&\ vacuum\ pump} = \frac{1}{\eta_{iso-s}}\ \dot{n}RT\ \frac{\gamma}{\gamma-1}\left(\left(\frac{p_{high}}{p_{low}}\right)^{\frac{\gamma-1}{\gamma}}-1\right) \tag{3}$$

$$\dot{W}_{turbine} = \eta_{iso-s}\ \dot{n}RT\ \frac{\gamma}{\gamma-1}\left(\left(\frac{p_{low}}{p_{high}}\right)^{\frac{\gamma-1}{\gamma}}-1\right) \tag{4}$$

$$\dot{W}_{pump} = \frac{1}{\eta_{iso-s}}\ \frac{\dot{m}}{\rho}\ (p_{high}-p_{low}) \tag{5}$$

$$Electrical\ consumption = \frac{\sum \dot{W}}{\dot{m}_{CO_2\ captured}} \tag{6}$$

where $\dot{W}$ the power rate (W), η_{iso-s} the isentropic efficiency, $\dot{n}$ the molar flow rate (mol.s^{-1}), R the ideal gas constant (=8.314 J.mol^{-1}.K^{-1}), T the temperature (K), γ the heat capacity ratio, p the pressure (Pa), $\dot{m}$ the mass flow rate (kg.s^{-1}), and ρ the density (kg.m^{-3}).

2.3 Economic analysis

Method from Turton *et al.* [89] is used to estimate the CAPEX and OPEX of the hybrid unit. This method relies on a reference cost adjusted by the Chemical Engineering Plant Cost Index (CEPCI) (equation (7)) to actualize the cost according to the inflation. For 2022 year, the average CEPCI index was equal to 816.0 [90].

$$C_{actual} = C_{reference}\left(\frac{I_{actual}}{I_{reference}}\right) \tag{7}$$

where C is the cost (€), and I the CEPCI index (-).

CAPEX is estimated via the calculation of the bare module cost (C_{BM}) equations (8) using the purchased equipment cost (C_p^0) which is evaluated by equation (9), and a bare module factor (F_{BM}) which include direct and indirect costs. If this factor is not given, a pressure factor (F_p) and a material factor (F_M) are used instead. The pressure factor can be obtained with equation (10) for a heat exchanger, or with equation (11) for a vessel. Material factor depends on the material used for the equipment and is equal to 1 for carbon steel. Equations (8) to (11) use different coefficients (K_i, B_i, C_i) given in Table 4 [89].

$$C_{BM} = C_p^0\ [B_1 + B_2\ F_P\ F_M] = C_p^0\ F_{BM} \tag{8}$$

$$\log_{10} C_p^0 = K_1 + K_2 \log_{10}(S) + K_3[\log_{10}(S)]^2 \tag{9}$$

$$\log_{10} F_{p,hx} = C_1 + C_2 \log_{10}(p) + C_3 [\log_{10}(p)]^2 \quad (10)$$

$$F_{p,vessel} = \frac{\frac{p\,D}{2\,St\,E - 1.2\,p} + CA}{t_{min}} \quad (11)$$

where C_p^0 is the purchased equipment cost corresponding to the atmospheric operating pressure and using carbon steel construction, S is the size of the equipment, p is the pressure (bar), D is the diameter (m), t_{min} is the minimum allowable vessel thickness (0.0063 m), CA is the corrosion allowance (0.00315 m), E is the weld efficiency (0.9), and St is the allowable stress for carbon steel (944 bar).

Table 4: Capital cost variable of components (: F_p = 1 for p < 5 barg).*

Equipment Type	K_1	K_2	K_3	B_1	B_2	F_{BM}	C_1	C_2	C_3
Compressors centrifugal	2.2897	1.3604	-0.1027	-	-	2.7	-	-	-
Floating head HX	4.8306	−0.8509	0.3187	1.63	1.66*	-	0.03881	-0.11272	0.08183
Turbines	2.2476	1.4965	-0.1618	-	-	1	-	-	-
Vertical towers and vessels	3.4974	0.4485	0.1074	2.25	1.82	-	-	-	-

The cost of the brazed aluminum heat exchanger and the vacuum pump cannot be estimated by the above equations since this exchanger is not reported in Turton *et al.* [89]. Instead, the costs are obtained by Aspen Economics software, for BAHX, using the volume of the exchanger calculated by the specific surface of the exchanger (2000 m^{-1}) [91] and the overall heat transfer coefficient (170 $W.m^{-2}.K^{-1}$) [54]. Subraveti et al. [92] gives regression for vacuum pump cost with volumetric inlet flow rate. The adsorbent cost was obtained by considering a price for the zeolite at 1.50 €.kg^{-1}.

CAPEX is obtained by summing the bare module cost of each equipment of the unit. In addition, a contingency cost and fees cost factor is added to the CAPEX calculation as a protection against the uncertainties of the cost estimation of each equipment. Contingency cost relies on numerous factors such as the completeness of the process flowsheet, or the reliability of the data used for the cost estimation. As a rule of thumb, 15% of bare module is used for contingency factor, and 3% is used as fees factor if no other data is available. Therefore, the final CAPEX calculation is given by equation (12) [89].

$$CAPEX = 1.18 \sum C_{BM} \quad (12)$$

The value obtained for CAPEX is annualized considering a lifetime of twenty-five years for the unit and the inflation rate. Equation (13) gives the annuity cost of the unit, depending on the inflation rate and the number of years.

$$CAPEX_a = CAPEX \frac{i(1+i)^n}{(1+i)^n - 1} \quad (13)$$

where $CAPEX_a$ is the annuity cost (€), i is the inflation rate (6.5%) [93] and n is the number of years of annuity interest.

OPEX is estimated from different factors listed in Table 5. These factors used Utility Cost (C_{UT}), Operating Labor Cost (C_{OL}) which is dependent of the country of the installation, and CAPEX. Equation (14) gives the complete formula to compute the OPEX.

$$OPEX = 1.235\,C_{UT} + 2.735\,C_{OL} + 0.280\,CAPEX \quad (14)$$

Finally, CO_2 capture cost can be calculated with the sum of the annuity of the CAPEX and the OPEX for one year of operation divided by the mass of CO_2 captured for one year (equation (15)).

$$Capture\ cost\ \left(€\ t_{CO_2}^{-1}\right) = (CAPEX_a + OPEX)/m_{CO_2\ captured} \quad (15)$$

Table 5 Base case assumptions for OPEX (Cooling water and labor cost from [93]; other coefficients from [89])

Parameter	Value
Utilities (C_{UT})	Electricity: Base case 100 €.MWh^{-1} with variation between 50 – 250 €.MWh^{-1} Cooling water: 0.025 € m^{-3}
Operating Labor Cost (C_{OL})	18 labors; 54,000 €.labor^{-1}.year^{-1}
Direct supervisory and clerical labor	0.18 C_{OL}
Maintenance and repairs	0.06 CAPEX
Operating supplies	0.15 (0.06 CAPEX)
Laboratory charges	0.15 C_{OL}
Patents and royalties	0.03 OPEX
Local taxes and insurance	0.032 CAPEX
Plant overhead costs	0.6 (1.18 C_{OL} + 0.06 CAPEX)
Administration costs	0.15 (1.18 C_{OL} + 0.06 CAPEX)
Distribution and selling costs	0.11 OPEX
Research and development	0.05 OPEX
Depreciation	0.10 CAPEX

3 Optimization

Simulation of VPSA and CPU in Aspen software requires the resolution of several thousand of equations leading to long simulation times. Optimizing each independent process using heuristic optimization algorithms (such as genetic algorithms, particle swarm optimization, simulated annealing, etc.) requires a significant number of simulation points, which would result in very slow resolution. In this work, the linking of VPSA and CPU requires calculating a steady-state point before optimizing the overall process. Surrogate models have been developed for both units, allowing to bypass Aspen simulations after having built robust and precise surrogate models and drastically reducing the required computational time. This methodology has been already used and validated in several research in the field of CO_2 capture processes [94–96].

Table 6 summarizes the input ranges used to build surrogate models for each process. The first part of the table includes the inputs for one VPSA unit, while the second part includes inputs for the CPU. The gas flow rate and its CO_2 concentration are included as inputs in each process since they are modified after the integration of the two units.

Table 6: Parameters for the surrogate models with lower and upper bounds (top part: VPSA, bottom part: CPU).

Parameters	**Definitions**	**Units**	**Lower bounds**	**Upper bounds**
$C_{CO2\text{-}FG}$	Inlet CO_2 concentration from flue gas	mol%	5	27
F_{FG}	Inlet flue gas flow rate of VPSA	Nm^3.h^{-1}	14,000	25,000
t_{ads}	Adsorption time	s	60	1500
t_{purge}	Purge time	s	10	1490
t_{equ}	Pressure equalizer time	s	10	50
F_{purge}	Purge flow rate	Nm^3.h^{-1}	100	20,000
p_{ads}	Adsorption pressure	bar	1.01325	3
P_{blow}	Blowdown pressure	bar	0.01	0.5
$C_{CO2\text{-}VPSA}$	Inlet CPU CO_2 concentration from VPSA	mol%	50	85
F_{VPSA}	Inlet CPU pre-concentrated flow rate from VPSA	Nm^3.h^{-1}	1,000	40,000
p_{C4}	Cold box pressure	bar	15	30
p_{V1}	Desorption column pressure	bar	9	17
p_{V2}	Second Joule-Thompson valve pressure	bar	7	14
α_1	Mass fraction towards desorption column	-	0.05	0.20
α_2	Mass fraction towards first JT valve	-	0.05	0.75

3.1 Surrogate model

Several mathematical models can be used to construct a surrogate model from simulation data. One of the simplest models widely used is the second-order polynomial approximation represented by the equation (26) [97,98].

$$\hat{f}(x,a,\alpha) = a_0 + \sum_{i=1}^{m} a_i x_i + \sum_{i=1}^{m} \alpha_{ii} x_i^2 + \sum_{i=1}^{m-1} \sum_{j=i+1}^{m} \alpha_{ij}\, x_i x_j \tag{16}$$

where $\hat{f}$ is the estimation of the response by the model, a and α the coefficients of the polynomial with a_0 being a constant, x the parameter (t_{ads}, t_{purge}, etc.) and m the number of parameters.

Unfortunately, for complex model, second-order polynomial approximation gives unsatisfactory results and require the use of other surrogate models. The Kriging method is a popular model for engineering problem, giving satisfactory results for the approximation of time-consuming simulation [98]. In a general way, Kriging models are composed of a deterministic term $F(x)$ (constant term, linear or quadratic model of parameters such as equation (16)), and a stochastic term $Z(x)$ (equation (17)). The main assumption of Kriging model is to consider a spatial correlation between the responses to the model (which implies to consider the responses as random variables, even if they come from a determinist simulation software), with a known correlation function between the variables. Therefore, the prediction of an unknow point can be done by using this correlation function, and the distance between the new point and the known points [98–100].

$$\hat{f}(x) = F(x) + Z(x) \tag{17}$$

Different correlation functions can be used to construct the Kriging model. A list of frequently employed functions is available in [98]. In this work, the choice of the correlation function is done empirically by testing different functions until satisfactory results are obtained.

The models were constructed following the flowchart in the Figure 5. A total of n $(= 100)$ points were generated with a Latin hypercube sampling using the Enhanced Stochastic Evolutionary algorithm [101], which allows for a semi-random distribution of points to ensure comprehensive coverage within the system bounds. The points were simulated with their respective tools and divided into two arrays to build the model with the first array (80% of data) and validate it with the second array (20% of data). The Surrogate Modelling Toolbox (SMT) [102] is used to construct both the surrogates of VPSA and CPU in Python.

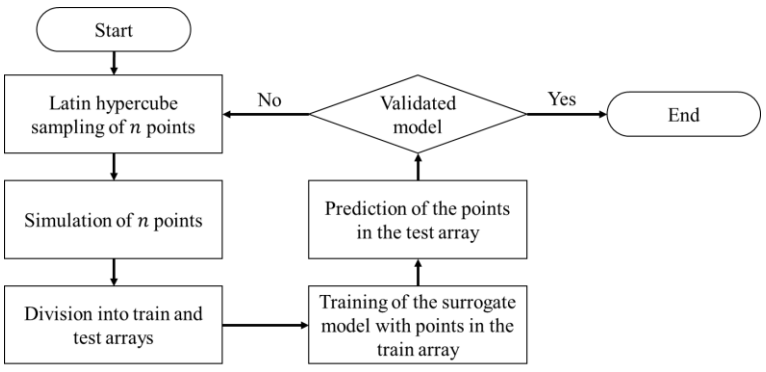

Figure 5: Algorithm for surrogate model creation.

For recovery and purity, the transformation described by (18) was applied to train the surrogate model with u the transformed data, z the training data, and ϵ a numerical perturbation equal to 0.0001. This transformation improves the robustness of the optimization procedure as stated by Beck et al. [103]. Recoveries and purities are obtained by applying the inverse transformation to the surrogate prediction.

For energy consumption, the transformation given by (19) was applied to avoid negative value from the surrogate model [104].

$$u = \log\left(\frac{z}{(1+\epsilon)1-z}\right) \tag{18}$$

$$u = \log(z+1) \tag{19}$$

Different indicators are used to quantify the fitting of the model with the validation points: coefficient of determination (R^2), mean absolute error (MAE), median absolute error (MedAE) and root mean squared error (RMSE) [97,98]. Equations 28 to 31 give the definition of the indicators.

$$R^2 = 1 - \frac{\sum_i^n (y_i - \widehat{y_i})^2}{\sum_i^n (y_i - \hat{y}_{mean})^2} \tag{20}$$

$$MAE = \frac{1}{n}\sum_i^n |y_i - \widehat{y_i}| \tag{21}$$

$$MedAE = median(|y_1 - \widehat{y_1}|, \dots, |y_n - \widehat{y_n}|) \tag{22}$$

$$RMSE = \sqrt{\frac{1}{n}\sum_i^n (y_i - \widehat{y_i})^2} \tag{23}$$

where y is a calculated value from the surrogate and $\hat{y}$ is a value from the Aspen simulations.

These indicators are divided by the difference between maximum and minimum of the values they are measuring. This normalization process results in dimensionless metrics, which can be better understood and compared across different scenarios. The model is considered validated when its R-squared value exceeds 97.5% and MedAE is less than 2% after normalization. MedAE was chosen among the different indicators due to the robustness of this indicator against outliners results.

3.2 VPSA and CPU linking.

Since the surrogate models of the two processes are independent, it is necessary to define an algorithm to link the two processes together. For each input array, a steady-state point will be calculated. Specifically, for a total flow rate and a concentration of CO_2 in the flue gas, when the inputs are fixed, the VPSA system produces a stream with a certain CO_2 concentration and flow rate that is processed in the CPU, and the CPU returns a gas flow containing residual CO_2 back to the VPSA inlet, which modifies the concentration and flow rate of the incoming stream to the VPSA (Figure 6). The system is considering to be in steady state when the variation in flow rate and concentration of the recycled stream between the CPU and the VPSA is smaller than a certain tolerance (set to 10^{-3} conserving concentration and flow rate unit). Section 3 of the supporting information present the cycle steady-state for inlet CO_2 concentration and flow rate of both unit.

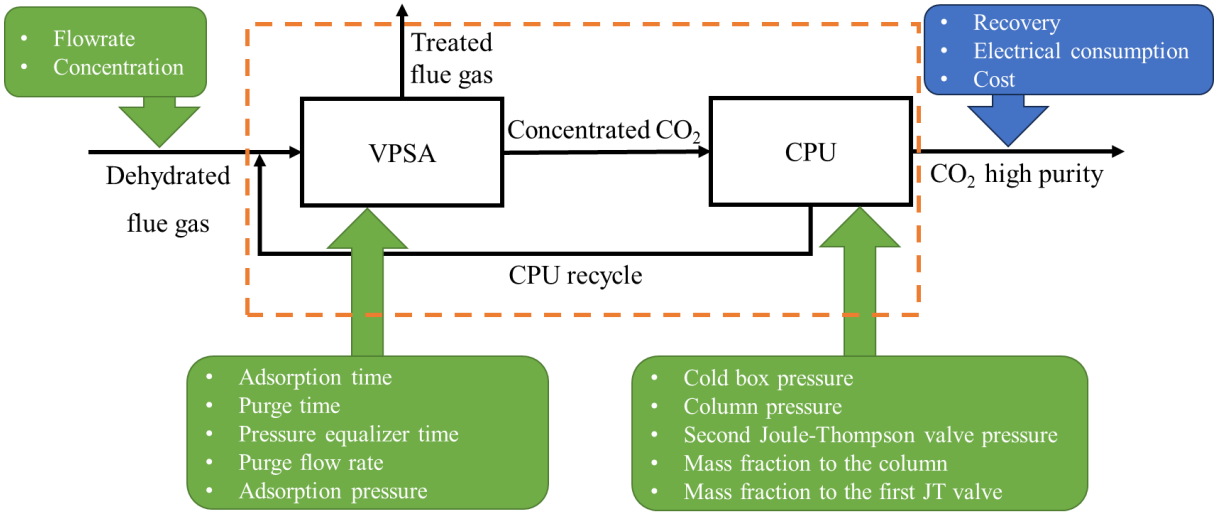

Figure 6: Linking VPSA+CPU with inputs and outputs.

The CO_2 recovery in the coupled process can be calculated as the quotient of the quantity of CO_2 captured as it emerges from the CPU in relation to the incoming CO_2 flow prior to its combination with the CPU recycle stream. Furthermore, the electrical consumption of the entire process is the sum of electrical consumption across its constituent processes, and the cost is intricately linked to the CAPEX and OPEX associated with each individual process.

3.3 Sensitivity analysis

Impacts of the different parameters on the complete unit were studied with a sensitivity analysis by computing the Sobol's total order indices for recovery and electrical consumption. Total order indices indicate relative importance of the different parameters with higher values for the most important parameters [105]. Estimation of indices use a Monte-Carlo process which requires the evaluation of CO_2 recovery and electrical consumption for multiple conditions. Surrogate modelling described in section 3.2 was used to evaluate the Sobol indices associated with the steady state point of global VPSA and CPU process.

The python library Salib [106] was used to evaluate the total order indices with the model of VPSA and CPU developed. To take into account the different constraints between the parameters of the two units, the analysis method was modified according to [107] with an acceptance-rejection sampling method allowing to use the Sobol method for non-rectangular domains ensuring a more accurate representation of the interplay between the parameters of the VPSA and CPU process.

3.4 Optimization algorithm

The objective of this study is to optimize a complex process with multiple objective functions, resulting in an irregular surface containing local minima. To address this challenge, U-NGSA-III (Unified non-dominated Sorting Genetic Algorithm III) genetic algorithm is chosen as it is known for its effectiveness in handling multi-objective problems [108]. U-NGSA-III builds upon the NGSA-III algorithm and enhances its performance through the introduction of new tournament pressure function that is the selection method of individuals.

NGSA-III, an evolution of NGSA-II, brings significant advances to the field of multi-objective optimization. It contains sophisticated mechanisms for preserving diversity, improving exploration and exploitation, and efficiently finding Pareto-optimal solutions. The algorithm uses non-dominated sorting to categorize solutions into distinct Pareto fronts, each representing a group of solutions that cannot be improved in one objective without affecting another.

By preserving diversity among solutions, U-NGSA-III provides a comprehensive representation of the trade-off space that allows decision makers to select the most appropriate solutions based on their preferences. The algorithm uses genetic operators such as selection, crossover, and mutation to steer the population toward the Pareto-optimal bounds, allowing efficient exploration and convergence to a diverse set of optimal solutions.

In summary, the choice of U-NGSA-III demonstrates its capability to address the challenges posed by multi-objective optimization, offering enhanced performance compared to its predecessor, NGSA-II. Its ability to efficiently explore the Pareto frontiers and maintain diversity among solutions makes it a valuable tool for tackling complex optimization tasks. To enhance the optimization of the VPSA and CPU, the Python library Pymoo [109] is employed.

4 Results and discussions

The surrogate models play a role in approximating and streamlining the complexities of the processes. Upon successful validation of the surrogate models, the subsequent step involves an analysis of process optimization for each component. This investigation culminates in a comprehensive assessment of the coupled process, encompassing both energy and economic considerations. This evaluation provides insights into the performance and sustainability of the integrated system, offering a complete perspective on its potential for real-world applications.

4.1 Surrogate models building and process analysis

4.1.1 VPSA process

A large number of successful simulations (namely 5280) have been performed to construct the surrogate model of the VPSA unit. To improve the calculation time, the Aspen Adsorption process is parallelized across the 8 cores of the PC. As explained in section 3.1, 4244 simulations have been used to construct the surrogate model, and 1056 simulations have been used to validate the model. A Kriging model was constructed using a polynomial function for the deterministic term, and the Matérn (3/2) kernel for the stochastic term. The model was then validated by using the different indicators presented in section 3.1. The indicators values for the different results are given in Table 7. CO_2 purity and CO_2 recovery of VPSA are defined in equation (1) and (2). Equation (6) gives electrical consumption calculation. Maximum energy consumption of compressor and maximum flow rate of vacuum pump are information used to calculate the CAPEX of the VPSA.

Table 7: Values of indicators for the surrogate model of VPSA.

	Purity$_{VPSA}$	**Recovery$_{VPSA}$**	**Electrical consumption**	**Maximum energy consumption of compressor**	**Maximum flow rate of vacuum pump**
R^2	97.5%	98.0%	97.8%	99.9%	98.1%
MAE	1.58%	1.39%	1.94%	0.27%	1.94%
RMSE	3.12%	3.71%	3.77%	5.07%	0.03%
MedAE	0.84%	1.57%	0.90%	0.14%	0.13%

The values obtained indicate a good representation of the validation points by the surrogate model, showing a R^2 value higher than 97.5%, and MedAE (and MAE) lower than 2%. Purity and maximum energy consumption of energy compressor have a good representation with high R^2, and low MAE and MedAE. For Purity, RMSE is higher than MAE and MedAE due to some outliner degrading the value of this indicator. Recovery and maximum flow rate of vacuum pump have a similar R^2 value, but other indicators are higher for the flow rate due to a larger error from the model. Energy consumption is the least well-represented result of the VPSA surrogate with a R^2 slightly higher the stop criterion described in 3.1. Nevertheless, the MedAE is similar to the purity which indicates that the value of R^2 is diminished by some outliner which is confirmed by the high value of RMSE.

The surrogate model of the VPSA unit was used to evaluate the pareto of VPSA recovery and purity at different CO_2 concentrations in the inlet flue gas for a flow rate of 14,000 $Nm^3.h^{-1}$. Pareto plot is given in Figure 7 for a CO_2 concentration of 5, 10 ,15 and 20%. As observed, the VPSA unit can reach high recovery for all CO_2 concentrations. The maximum CO_2 purity obtained in the unit increases with the inlet CO_2 concentration. For all CO_2 inlet concentrations, a sharp decrease of purity is observed as the VPSA recovery increases. The decrease of purity is stepper between 95 and 100% recovery for the VPSA due to an increase of purge time to recover all the CO_2 adsorbed.

An observation reveals that, at a 5% CO_2 concentration level, only recoveries lower than 85% allow to reach the value of 50 mol% of CO_2 for the CPU. This implies that the current configuration may render this flue gas treatment impossible to reach the target of 95% recovery and purity. Nevertheless, it is imperative to account for the impact of the CPU recycle, as it has the potential to increase the feed stream's concentration, thereby increasing the possibility of achieving higher purity levels at the VPSA's outlet.

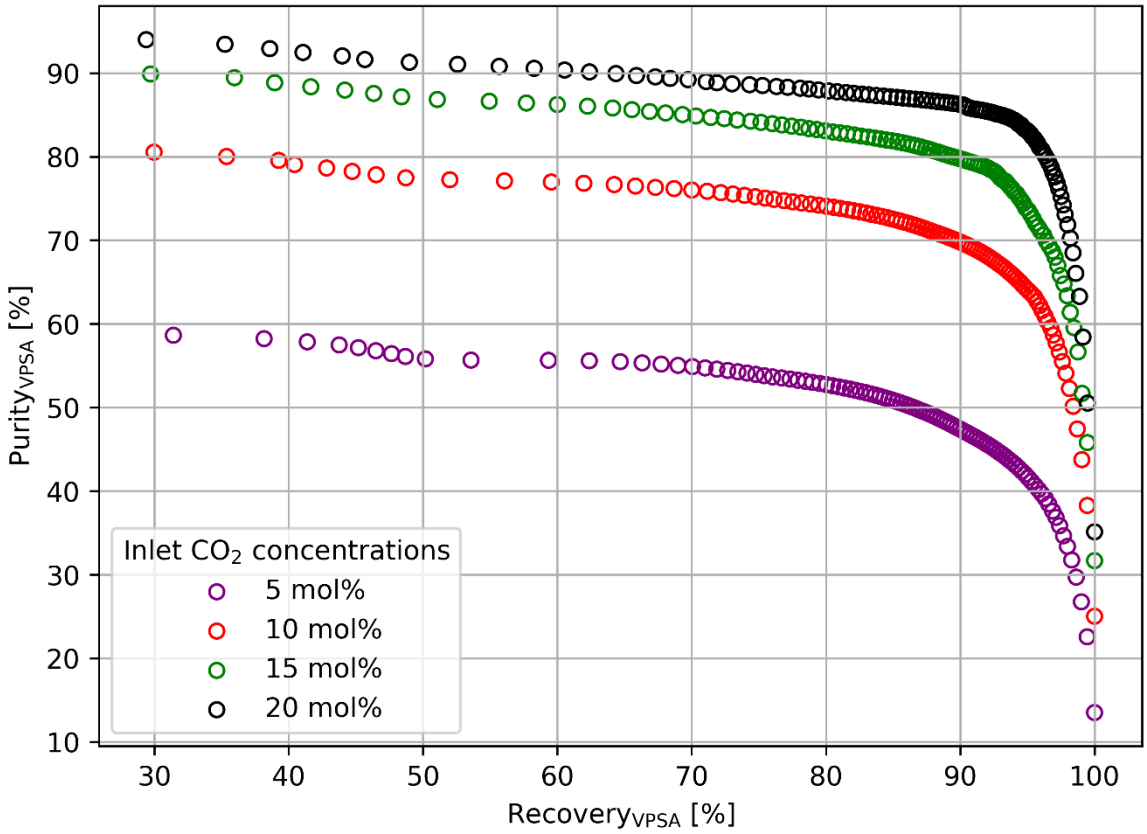

Figure 7: Pareto plot of the VPSA unit for different CO_2 molar fractions in the flue gas with a flow rate of 14,000 $Nm^3.h^{-1}$.

4.1.2 CPU process

Among the CPU inputs used (detailed in Table 6) to build the surrogate of the CPU process, some of them cannot be considered because they give results outside of the constraints. Among 24,200 points tested, 2,628 have satisfied the constraints. Thus 2102 points are used to build the surrogate model and 526 have been used to validate the model. A Kriging model was constructed using a polynomial function for the deterministic term, and the Gaussian for the stochastic term. The model was then validated by using the different indicators presented in section 3.1. The indicators values for the different results are given in Table 8. Equation (6) gives electrical consumption calculation for the CPU. Flow rate and CO_2 concentration to VPSA are the information of the recycle stream that go to VPSA. CAPEX is calculated for the complete CPU process and the cooling water flow rate is part of utility in the OPEX.

606 *Table 8: Value of indicators for the surrogate model of CPU.*

	Electrical consumption	Flow rate to VPSA	CO_2 concentration to VPSA	CAPEX	Cooling water
R^2	99.9%	99.9%	99.9%	99.9%	99.9%
MAE	0.1%	0.1%	0.1%	0.1%	0.6%
RMSE	0.5%	0.1%	0.1%	0.2%	1.0%
MedAE	0.1%	0.1%	0.1%	0.1%	0.3%

607

608 The calculated indicators show an excellent mathematical representation of the CPU modelled in Aspen
609 Plus® V14. During the data analysis, attention was given to ensure an appropriate distribution of points
610 within the defined bounds for various parameters. This analysis revealed distinct physical constraints
611 associated with relationships between two specific parameters. Figure 8 highlights three pairs of
612 parameters that exhibit these physical limits. It shows comparisons among the 24,200 simulations,
613 categorizing the points that either meet or fail to meet these constraints.

614 Figure 8 (a) illustrates the relationship between the cold box pressure and the column pressure. The
615 limit in the upper-left corner is associated with insufficient cooling input into the system, while the one
616 in the bottom-right corner is linked to excessive expansion between the two pressures, causing the stream
617 to drop below -54 °C. Figure 8 (b) relates column pressure to the mass fraction returning to it. If the
618 pressure is too high and the CO_2 vapor flow at the bottom of the column is too low, this leads to
619 hydrodynamic column issues. Figure 8 (c) connects the pressure of the second Joule-Thompson
620 expansion with the mass fraction going to the first Joule-Thompson expansion. If there is insufficient
621 flow to this expansion and the pressure drop in the second expansion is too low, there is a lack of cold
622 flow to the cold box. These limits are incorporated during optimization by adding constraints to prevent
623 the system from going beyond what is physically possible.

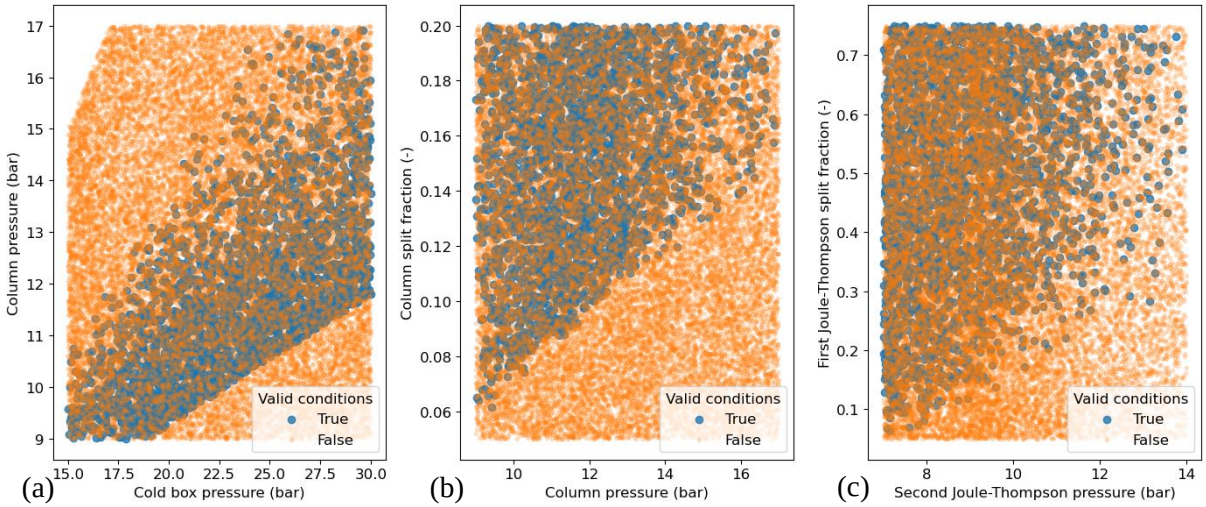

624
625 *Figure 8: Physical limits driven by conditions in the process between parameters (a) Cold box pressure/Column pressure –*
626 *(b) Column pressure/Column split fraction – (c) Second Joule-Thompson pressure/First Joule-Thompson split fraction.*

627 Optimizing the CPU with an inlet flow rate of 10,000 $Nm^3.h^{-1}$ and varying concentrations ranging from
628 50 to 85 mol% CO_2 demonstrates an interesting trend (Figure 9). As the CO_2 concentration in the feed
629 from the VPSA increases, the electrical consumption is decreasing, which presents a promising energy-
630 saving prospect for the CPU. These findings are in line with the broader observations made across
631 various capture units, all of which point towards reduced electrical consumption as CO_2 concentrations
632 rise.

633 Furthermore, an interesting correlation emerges in terms of the recycled flow. This flow is directly
634 linked to the decreasing concentration of nitrogen within the system. The reducing nitrogen

concentration implies a reduction in the volume of non-condensable components exiting the cold box during the flash separation process from the liquid CO_2.

By definition, the higher the concentration of CO_2 in the VPSA feed, the more energetically advantageous it becomes for the CPU. However, in our quest for optimization, it remains crucial to determine the precise threshold at which these two processes, VPSA and CPU, reach their optimal balance, ensuring the most efficient and energy-effective operation.

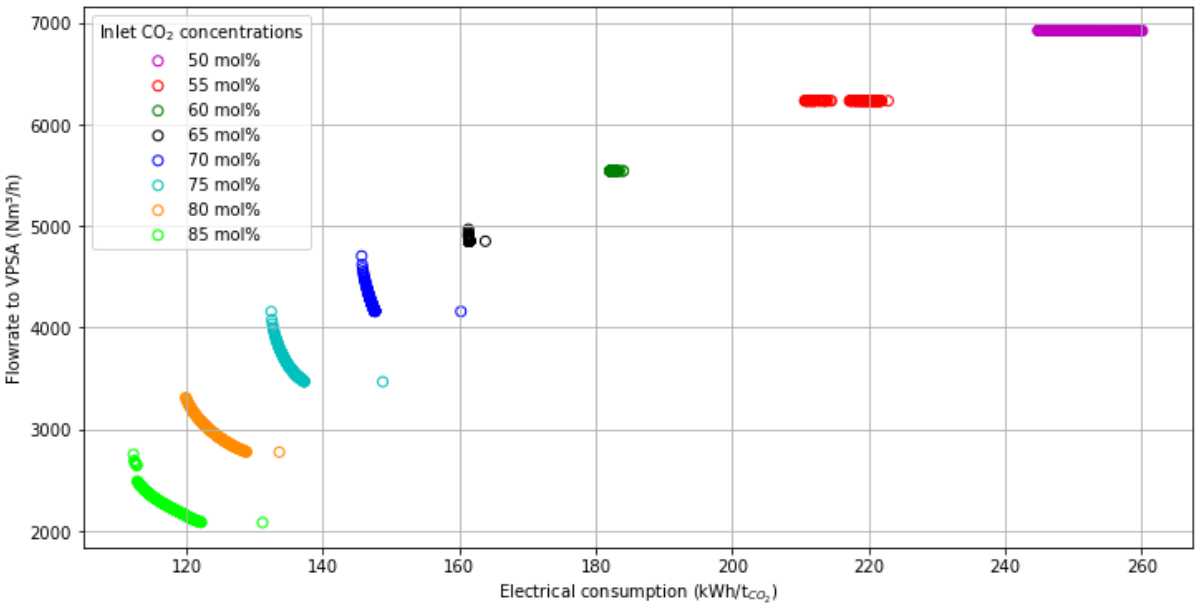

Figure 9: Pareto plot of optimization between electrical consumption and flow rate to VPSA for a stream of 10,000 $Nm^3.h^{-1}$ at different inlet CO_2 concentrations.

After analyzing the parameters used for optimizing CPU performance, some interesting trends emerge regarding electricity consumption: (i) when the pressure in the cold box decreases, the electrical consumption also decreases, while the flow rate towards the VPSA unit increases, (ii) the cooling temperature of the flue gas is constant and (iii) thanks to the higher pressures operation, more CO_2 turns into a liquid form resulting in a lower flow rate to the VPSA unit.

The column pressure tends to approach its limit to the cold box pressure reducing the energy needed to recompress vapor from the column. Another key factor of optimization involves the minimization of the mass fraction directed towards the column for the desorption. This approach ensures an optimal flow rate to operate the column while simultaneously mitigating product loss, particularly with regards to CO_2 recirculation.

Additionally, optimizing the performance of the second Joule-Thompson valve is also important for achieving the lowest electrical consumption while maintaining a robust refrigeration output. Simultaneously, minimizing the mass fraction allocated to the first Joule-Thompson valve, which operates at the lowest pressure, is paramount for achieving optimal electrical consumption.

In conclusion, this comprehensive analysis reveals intricate relationships between various parameters and electrical consumption in CPU optimization. These findings highlight the importance of carefully tuning these parameters to strike a balance between process performance and energy efficiency.

4.2 Sensitivity analysis

Sobol's total order indices for the coupling were determined for CO_2 recovery and energy consumption with surrogate models. Results obtained are represented in Figure 10 for different CO_2 concentrations

in the flue gas. Uncertainties indices for the 5% case are higher due to the purity requirement of 50% for the CPU leading to numerous samples out of bounds compared to higher CO_2 concentration.

For all the CO_2 concentrations, adsorption and purge times are two important parameters with high indices (around 0.8) for both recovery and energy consumption except for the 20% case where the indices of adsorption time are lower for recovery than energy consumption. The link with purge time is straightforward since an increase of purge time will lead to a better desorption of CO_2 and thus a better recovery but also to an increase of energy consumption and decrease of purity due to the nitrogen flux which can affect the CPU performance. Adsorption time also change the amount of CO_2 inside the adsorption bed which can influence recovery and purity of VPSA unit. Adsorption time and purge time can also have a combined effect since blowdown time is equal to adsorption time less purge time. A higher blowdown time can increase the amount of CO_2 recovered from the adsorption bed. Nevertheless, total order indices do not give any information on interactions between parameters. As excepted, equalization time only affects the results for the 5% case and has very low indices for higher CO_2 concentrations, this step being dedicated to energy recovery. Due to the minimum purity required for CPU, the adsorption pressure for the 5% case is always close to 3 bar which can explain why the pressure equalization is more important in this case to reduce the energy consumption. The effect on recovery can be caused by the change of flow rate in the VPSA inlet due to the equalization time (see section 2.1.1). This effect could be less important for higher CO_2 concentrations. Effect of adsorption pressure on recovery and energy consumption can easily be interpreted as the increase of adsorbed amount in zeolite 13X with the increase of pressure which increase the recovery. In addition, the rise of pressure increases the power of the feed compressor in the VPSA unit. The effect of adsorption pressure on recovery decreases as the CO_2 concentration in the flue gas increases due to the shape of adsorption isotherms having a plateau at higher partial pressure of CO_2. Therefore, an increase of adsorption pressure is less impacting on the performance of the VPSA unit. Blowdown pressure is more important than adsorption pressure for both recovery and purity. In fact, this parameter is as important as the adsorption time or purge time. The impact of blowdown pressure on recovery can be explained by the sharp change of adsorbed amount at low pressure on the CO_2 adsorption isotherm of zeolite 13X. Therefore, low blowdown pressure leads to higher working capacity in the bed which increases the performance of the VPSA process. Nevertheless, decreasing blowdown pressure increases the energy consumption of the process. Since the efficiency of the vacuum pump is lower than the efficiency of compressor, the effect of blowdown pressure is more important on the energy consumption of the process than adsorption pressure. Purge flow rate is an important parameter for all the CO_2 concentration with indices higher than adsorption pressure. An increase of purge flow rate allows to recover more CO_2 from the adsorption column but decrease the purity. This affects the performance of the CPU and increase the flow rate across the vacuum pump of the VPSA unit and the CPU compressors which increase the overall energy consumption.

From the CPU side, cold box pressure is one of the key variables at 5% CO_2 concentration (0.6) and becomes less important at higher CO_2 concentration. The effect of this parameter on energy consumption is easily understood since a rise of pressure increases the energy consumed by the multi-stage compressor of the CPU. This pressure also determines the liquid-vapor equilibrium of the mixture in the flash separator in the CPU, and thus modify the recirculated flow send to the VPSA units. This is particularly critical for the 5% case where the recirculated flow can strongly enhance the performance of VPSA by increasing the CO_2 concentration of the flue gas. The desorption pressure has a constant effect (0.15) on recovery and energy consumption for all the CO_2 concentrations studied. Desorption pressure directly affects the compression ratio between compressors C3 and C4 (see Figure 4) and thus energy consumption of the CPU. This pressure can also slightly change the vaporization temperature in the desorption column, impacting the recirculating flux to the exchanger and the overall equilibrium in the flash which could explain the impact on recovery. The Joule-Thompson expansion pressure is one of the less impacting parameters (less than 0.1). This expansion is used to provide the cold source for the CPU, but the pressure of this step does not affect the overall efficiency of the coupling between

VPSA and CPU. The two last parameters are the fraction from the desorption column used for stripping (α_1) and the fraction send to the Joule-Thompson valve (α_2). The first fraction plays an important role in the recovery and energy consumption of the coupling with an index of more than 0.2 which is as important as cold box pressure for 10, 15 and 20% case. The amount of gas used in the desorption column will directly impact the energy consumption of the CPU with an increase of flow rate in compressor C4 (Figure 4), and will indirectly impact the recovery and energy consumption by changing the liquid-vapor equilibrium in the flash unit. Parameter α_2 has a low and similar impact to the pressure of the Joule-Thompson expansion and will affect the cold source of the CPU unit.

In a general way, recoveries and energy consumptions seem to be mainly driven by the adsorption time, purge time, and blowdown pressure (indices around 0.6). For higher CO_2 concentration the other main variables are adsorption pressure, purge flow rate, cold box pressure, desorption pressure, and α_1 with indices between 0.2 and 0.4. Equalization time, Joule-Thompson expansion pressure and α_2 have a limited effect on the recoveries and energy consumptions of this unit. These variables could be eliminated in a parametric study with a limited impact if a similar unit must be studied.

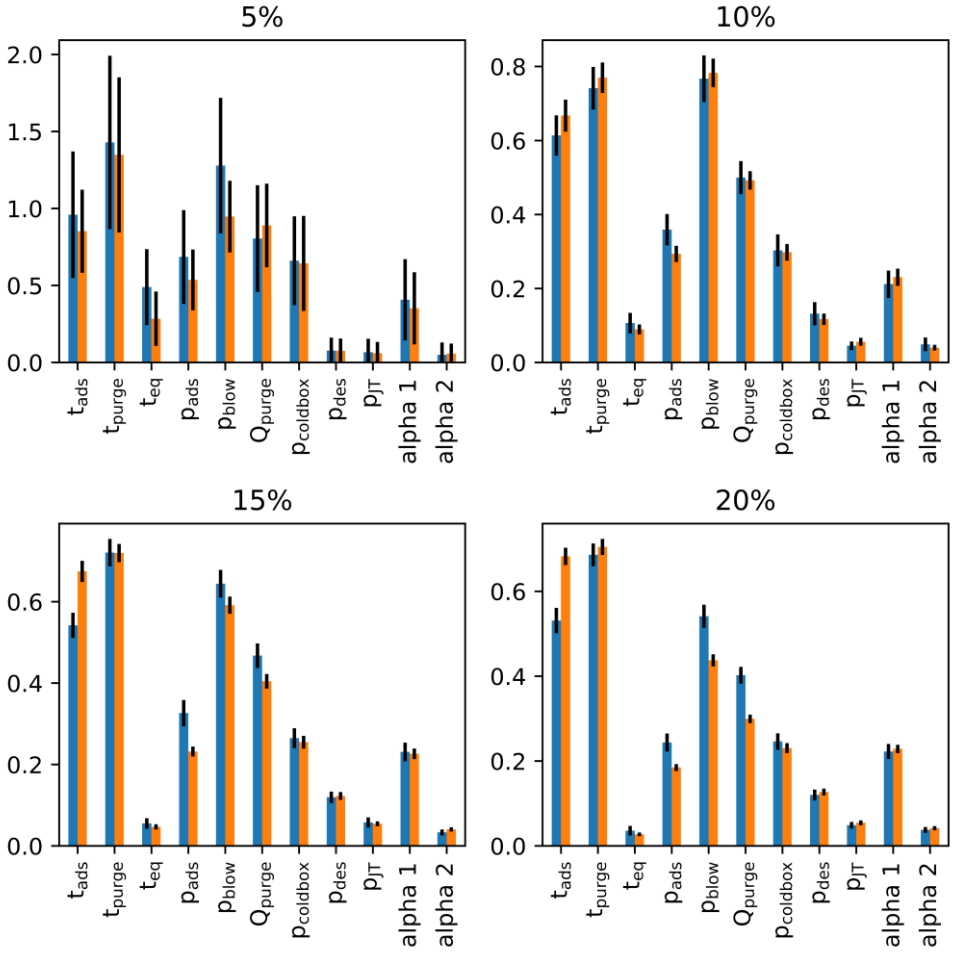

Figure 10: Sobol's total order indices determined for recovery (blue) and energy consumption (orange) obtained for the coupling of VPSA and CPU with a CO_2 molar fraction in the flue gas of 5, 10, 15 and 20% for a flow rate of 70,000 $Nm^3.h^{-1}$.

4.3 Multi-objective optimization of the complete process

With both surrogate models now effectively established and validated, the optimization for the VPSA + CPU coupling can be performed. The focus will be on optimizing both recovery and electrical consumption. The primary objective is to maximize the recovery process while concurrently minimizing electrical consumption. A range of inlet concentrations, varying from 5 to 20 mol% with 5 mol% increments, for a flue gas of 70,000 $Nm^3.h^{-1}$, will be examined.

Figure 11 displays the results of the combined process optimization. The higher the concentration of CO_2 in the inlet flue gas, the less electricity is consumed. To achieve the highest recovery rates, it is necessary to increase electrical consumption. As the results demonstrate, recovery rates approaching 99% are achievable thanks to VPSA technology. Therefore, it is reasonable to inquire about the desired recovery rate. To address this question, it is essential to consider the electricity prices and carbon taxes in order to determine the optimum recovery point. Gaps in the pareto front come from the algorithm approach of the NGSA-III that provides results close to the optimal point. In addition, the pareto plot between energy consumption and productivity is represented in Section 4 of Supporting Information.

A noticeable discrepancy in electrical consumption is observed for the 5% concentration compared to the others. This variance is attributed to a more substantial compression of flue gases at the entrance of the VPSA, and low blowdown pressure to increase the working capacity of the VPSA pilot enhancing adsorption of CO_2 with the same amount of adsorbent. Furthermore, the requirement to achieve a 50% CO_2 purity imposes operating conditions that are not particularly energy-optimal for the VPSA. This constraint also results in an inability to attain a 99% recovery, as it is no longer valid beyond a 95.5% recovery threshold.

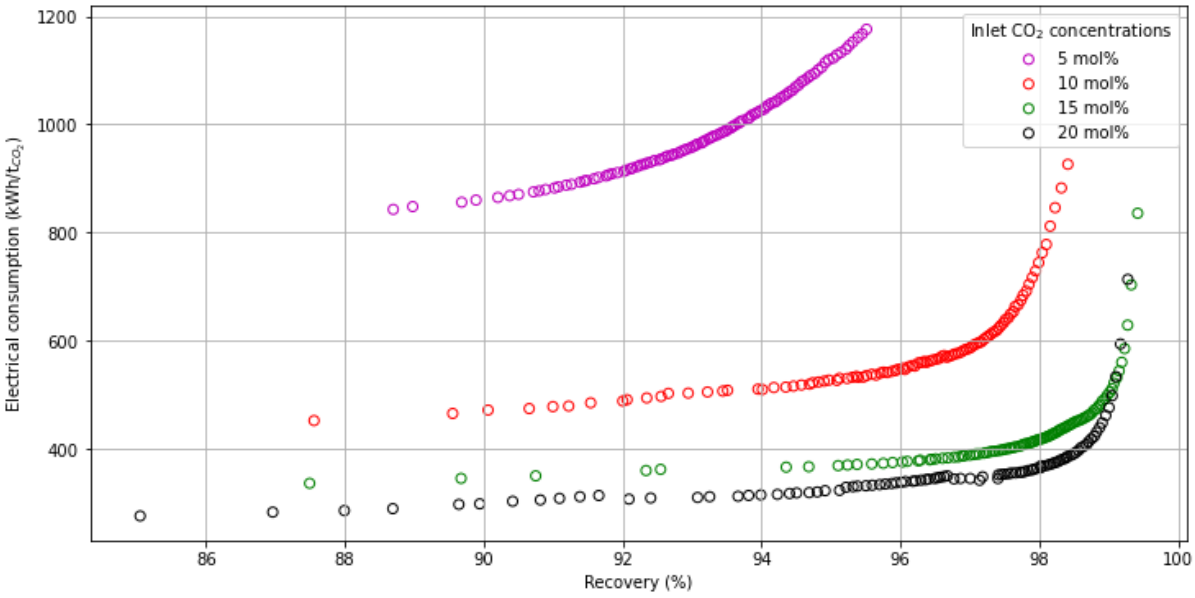

Figure 11: Pareto plot of the optimization between electrical consumption and global CO_2 recovery for different inlet CO_2 concentrations.

When analyzing the variation of CPU parameters, it becomes evident that the pressure in the cold box is relatively low, between 17 and 22 bar, compared to the CPU-alone optimization. This observation suggests that it is advantageous to increase the flow rate directed towards the VPSA unit, concurrently enhancing the concentration of CO_2 in this stream. Consequently, this strategy leads to a greater reduction in consumption on the VPSA side, thanks to a stream that is enriched in CO_2 compared to the initial flue gas, despite an overall increase in the flow through the VPSA.

In general, the other parameters exhibit similar trends as seen in the standalone CPU optimization, although with relatively consistent outcomes throughout the recovery evolution. Thus, it is likely more relevant to focus on optimizing the VPSA, which appears to maintain a relatively stable operational point. A comprehensive study of the parameter impact will subsequently be conducted to further delve into this discussion.

By analyzing the purity of the output from the VPSA in relation to recovery (Figure 12), it becomes evident that purity is highest at lower recovery levels which correspond to lower electrical consumption rates. This phenomenon is characteristic of VPSA systems, where an increase in purity is accompanied

by a decrease in recovery. To achieve recovery exceeding 90%, it is therefore necessary to reduce the purity at the VPSA output, resulting in an increase in CPU-side consumption. The constraint of minimum 50% of purity from the VPSA unit is also visible in Figure 12, especially for the 5% case.

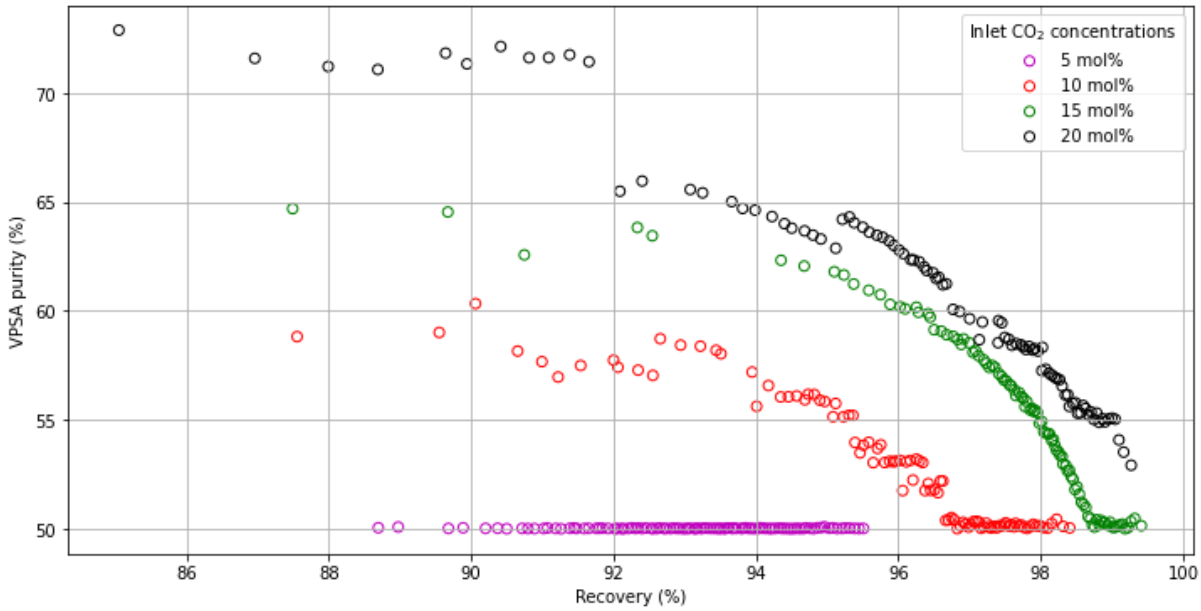

Figure 12: CO_2 purity of the output from the VPSA as a function of CO_2 recovery for different inlet CO_2 concentrations.

The volumetric flow rate entering the CPU experiences an upward trend corresponding to increasing concentrations (Table 9). This increment is attributable to the increase of CO_2 amount in the flue gas which increase the volume of gas sent to the CPU unit for a same recovery and purity of the VPSA unit. In addition, a correlation between flow rate and recovery can be found, where a higher recovery results in more CO_2 being captured by the VPSA and subsequently directed to the CPU.

Table 9: Inlet and outlet from VPSA and CPU for different inlet CO_2 concentrations.

		5 mol%		**10 mol%**		**15 mol%**		**20 mol%**	
		Min	Max	Min	Max	Min	Max	Min	Max
CPU inlet flow rate	$Nm^3.h^{-1}$	6,960	7,570	11,960	16,940	16,600	28,850	18,950	38,450
Recycled flow rate to VPSA	$Nm^3.h^{-1}$	6,000	7,170	9,860	16,180	9,200	22,000	10,200	30,000
VPSA inlet concentration	CO_2 mol%	7.6	7.8	13.6	14.9	18.6	21.6	22.4	26.2

The recycled stream directed back to the VPSA is enriched with a concentration ranging from 30 to 50 mol%. The post-cold box temperature of the flue gas is carefully set to adhere to the minimal temperature threshold, ensuring the prevention of dry ice formation. Consequently, the liquid-vapor equilibrium at the flash is mainly influenced by the pressure of the flue gas. At lower pressures, the vapor phase exhibits the highest concentration of CO_2. The CO_2 concentration in the gas stream entering the CPU from the VPSA plays a fundamental role in determining, at a given pressure, the volumetric flow rate returning to the VPSA (Table 9). This nuanced understanding of the interdependencies between pressure, temperature, and concentration elucidates the intricate dynamics of the system, offering valuable insights for further optimization and refinement.

Hence, the concentration at the VPSA inlet is enhanced through this recycling stream (Table 9). This augmentation significantly improves the VPSA performance by elevating the partial pressure of CO_2, thereby improving the adsorption process. This enhancement permits to achieve recoveries exceeding 90% across all cases, consequently attaining a purity of 50% at the VPSA outlet.

An interesting aspect that emerges from this optimization work is that there are several points beyond the conventional recovery rate of 90%. A more detailed study of specific scenarios can be conducted by considering different recovery levels such as 90%, 92.5% and 95%. Figure 13 compares the electrical consumption from VPSA and that from the CPU. For the 5 mol% case, VPSA consumes significantly more than the CPU, accounting for around 60% of the total consumption. For 10 and 15 mol% recovery, the ratio is smaller and close to 50%. For the 20 mol%, the situation reverses, with the CPU becoming the more consumptive component. Furthermore, as the desired recovery rate increases, the ratio of CPU consumption to VPSA consumption also rises. This observation is ultimately linked to the purity of the output stream from VPSA, which decreases, as presented in Figure 12.

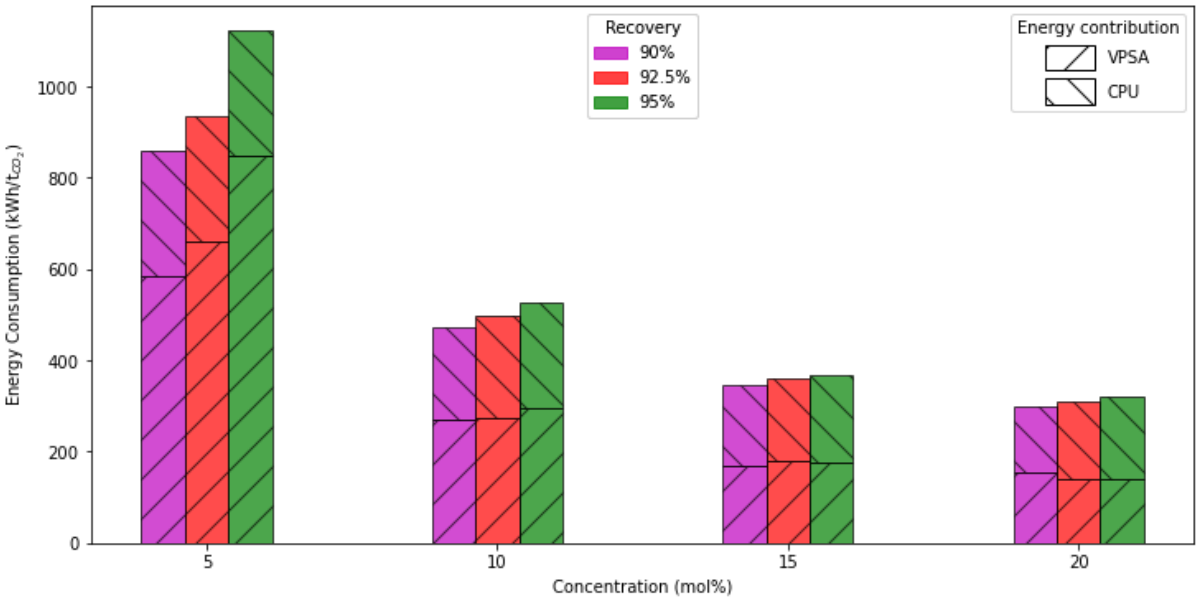

Figure 13: Energy consumption of VPSA and CPU at several recovery for different inlet CO_2 concentrations.

4.3.1 Techno-economic analysis

The main objective of this work is minimizing the electrical consumption of the entire VPSA-CPU process. For this type of installations, operational costs significantly outweigh fixed annual costs. Nevertheless, it is imperative to conduct cost estimations to assess the feasibility of this process and enable meaningful comparisons with other methods.

Being highly dependent on electrical consumption, the price of electricity per kilowatt-hour will have a substantial impact on the cost. Carbon taxation, on the other hand, serves to isolate an optimal recovery point since it is directly linked to the quantity of emitted CO_2.

Figure 14 illustrates the capture costs as a function of CO_2 recovery. It is noticeable that there is a substantial gap between the costs for a flue gas concentration of 5 CO_2 mol% compared to the other concentrations. These costs follow the same trend as the electrical consumption curves. This is attributed to the significant proportion of the cost allocated to electrical consumption, accounting for more than 90% when electricity costs are considered equal to 100 €.MWh^{-1}. Similar to Figure 11, the difference is more pronounced for the 5% concentration since the costs are primarily driven by electrical consumption. As for electricity consumption, the cost sharply increases when the recovery approaches 99% due to the diminution of purity.

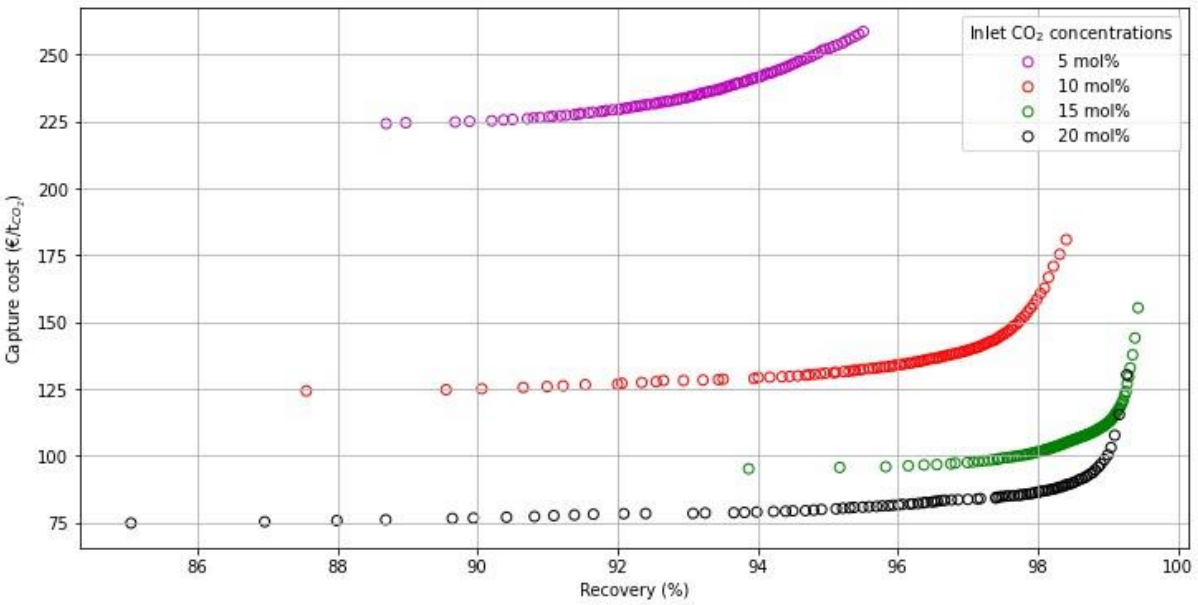

Figure 14: CO_2 capture cost as a function of CO_2 recovery for different inlet CO_2 concentrations.

Figure 15 illustrates the diverse contributions of CAPEX and OPEX for both the VPSA and CPU units. In the overall cost structure, the CAPEX component constitutes a noteworthy portion, ranging between 5% and 10%. Notably, for the 5% concentration, the VPSA CAPEX surpasses the CPU one, which differs from other cases where the CPU's CAPEX stands as the most substantial contribution.

Turning attention to OPEX, a pronounced pattern emerges. The preeminent share of costs emanates from the VPSA, particularly within the concentration range of 5% to 10%. However, as the concentration escalates to 15 and 20%, the CPU assumes a dominant role in driving overall operational expenses. This shift in the cost dynamics can be attributed to the pronounced impact of electricity costs within the operational expenditure framework.

Understanding the nuanced interplay between CAPEX and OPEX contributions is crucial for optimizing the economic viability of the integrated VPSA and CPU system. It not only underscores the financial implications of different concentration scenarios but also emphasizes the importance of addressing specific cost drivers, particularly electricity expenses, to enhance the economic efficiency of the overall carbon capture process.

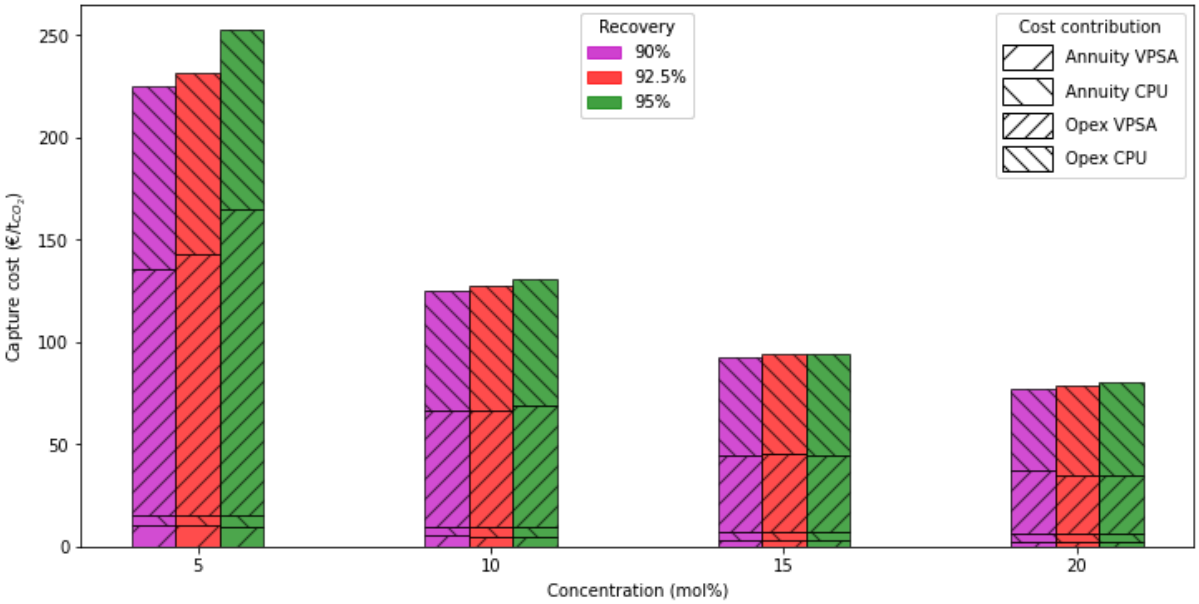

Figure 15: CAPEX annualized (annuity) and OPEX contribution of VPSA and CPU at several for different inlet CO_2 concentrations.

Considering the carbon tax for uncaptured CO_2, an optimum can be determined for a CO_2 recovery value. Per ton of CO_2, the total cost, including the CO_2 capture costs and the carbon tax, can therefore be calculated as follows:

$$Total\ cost = \frac{CO_2\ recovery}{100} CO_2\ capture\ cost + \frac{(100 - CO_2\ recovery)}{100} carbon\ tax \quad (24)$$

The evolution of total cost as a function of recovery and carbon tax for various concentrations is presented in Figure 16. During 2023, carbon tax of EU-ETS varying between 77.39 and 100.34 €.t_{CO2}^{-1} [110]. The interval of the carbon tax is considered between 70 to 130 €.t_{CO2}^{-1}. Different scenarios emerge based on the flue gas CO_2 concentration to determine the financially optimal recovery. Considering an electricity price of 100 €.MWh^{-1}, the cost optimum is below 90% recovery for the different cases. As the carbon tax rate increases, the optimum recovery rate tends to approach higher levels.

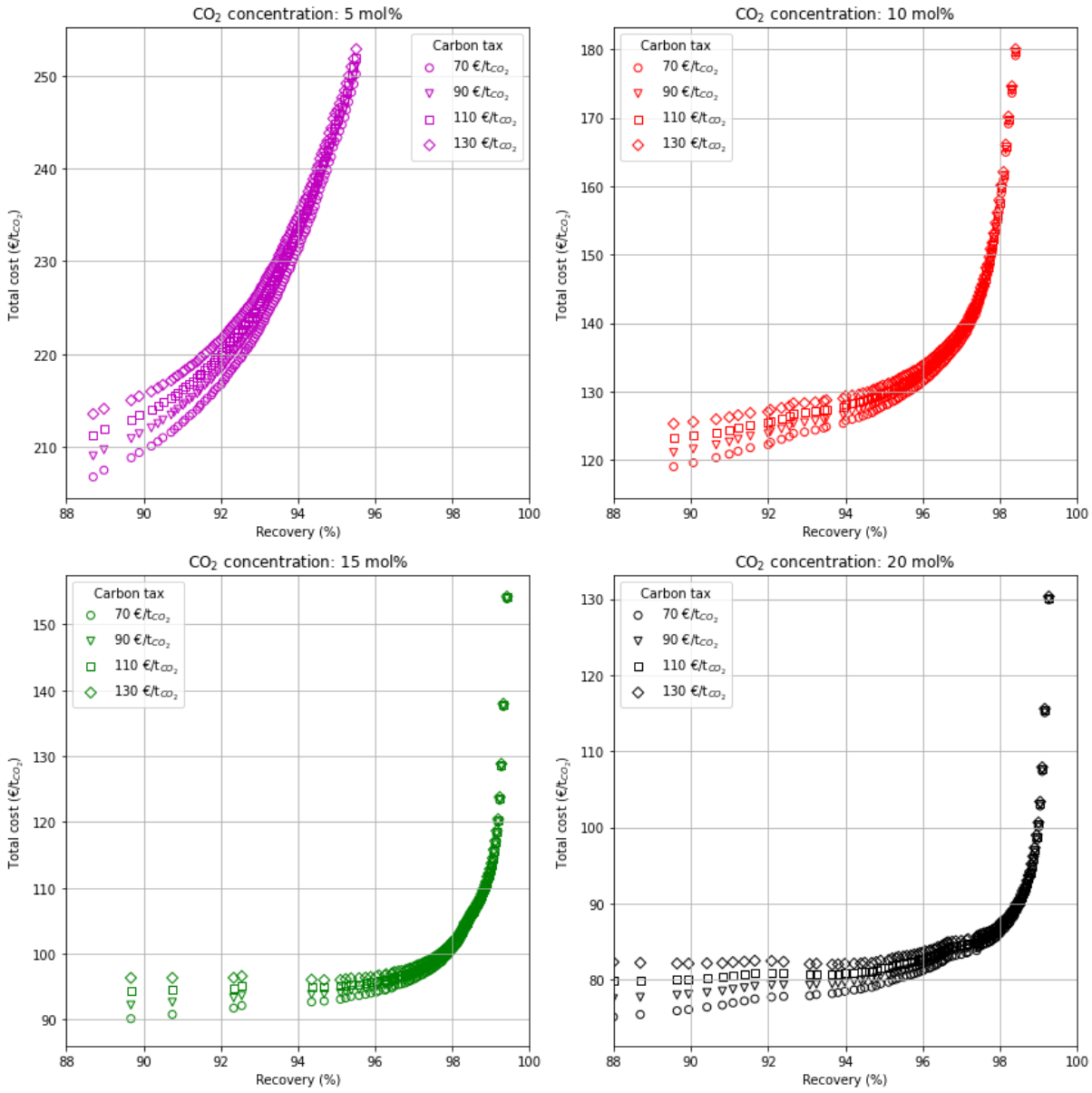

Figure 16: Evolution of total cost as a function of CO_2 recovery and carbon tax for different inlet CO_2 concentrations (electricity price: 100 €.MWh^{-1}).

4.3.2 Electricity price variation

The fluctuation of electricity prices is a topic of utmost importance in the fields of energy and economics. This variability is influenced by a multitude of complex factors, including the availability of energy resources, the production costs, the demand, the government policies, the international energy market fluctuations, and the technological advancements. In this study, the process under investigation consumes only electricity. To examine the impact of electricity prices on the total process cost, it was varied from 50 to 200 €/MWh. Electricity price variation will have an important impact on the optimum recovery at minimal total cost. Figure 17 displays the minimum total cost according to equation (24) as a function of carbon tax and CO_2 concentration within this range of electricity prices. Notably, the optimal recovery rate is higher for lower electricity prices.

For the 5% concentration, this technology demonstrates a substantial cost disadvantage over the carbon tax. Consequently, it is presently not prudent to consider such installations for concentrations at this low level. This process become interesting for 10% concentration for a high carbon tax (> 130 €/t_{CO2}) and a

low electricity price (< 50 €/MWh). However, for other concentrations, if the electricity cost remains below 100 €.MWh^{-1} and the carbon tax is at least 100 €.t_{CO2}^{-1}, this technology proves to be relatively compelling. Furthermore, achieving a recovery rate exceeding 90% remains economically viable and attractive.

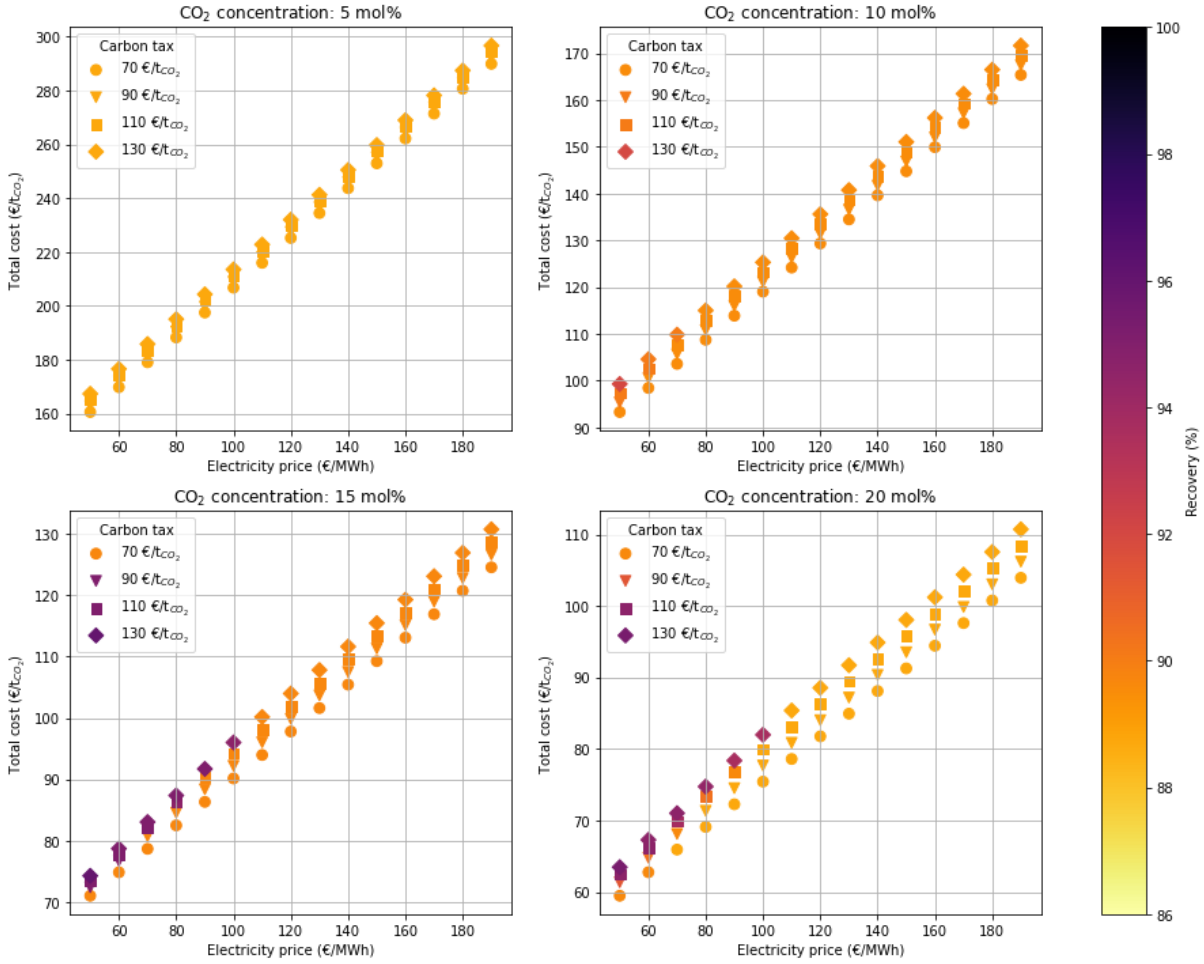

Figure 17: Optimum total cost for several carbon tax in function of the electricity price and the CO_2 inlet concentrations.

4.3.3 Environmental impact of the electricity source

The environmental impact, in terms of CO_2 avoided, of a fully electric carbon capture unit is assessed considering diverse electricity sources. The incorporation of an integrated electric-driven carbon capture system signifies a pivotal advancement in sustainable technology. The comprehensive analysis encompasses an evaluation of the environmental ramifications associated with the electricity sources powering the carbon capture unit. This investigation serves to elucidate the broader environmental implications of deploying electric-based carbon capture technologies and emphasizes the critical significance of opting for environmentally sound energy sources to augment the overall sustainability of carbon capture processes. Conventional sources, including coal, natural gas as well as renewable alternatives such as wind are scrutinized. Furthermore, the European electricity mix (ENTSO-E) is considered in the analysis to assess the impact on current energy producers. Solar production emissions are close to the wind production emissions.

Figure 18 illustrates the dynamic trajectory of *CO_2 avoided*, representing the captured CO_2 minus the emissions associated with electricity production. This is normalized against the total quantity of CO_2 present in the initial flue gases.

$$CO_2\ avoided = \frac{CO_2\ captured - CO_2\ emitted\ by\ power\ production}{CO_2\ flue\ gas} \quad (25)$$

Across various concentrations, the influence of a purely wind-powered source on recovery is negligible, resulting in *CO_2 avoided* levels closely mirroring the recovery rates. Emissions linked to the European electricity mix closely approximate those of a natural gas power plant. The trend in *CO_2 avoided* is capped at over 98% for different concentrations. Notably, at a 90% CO_2 recovery rate, there is a discernible decrease of 34%, 18%, 13%, and 11% attributable to emissions from the European mix for concentrations ranging from 5% to 20%, respectively. For the different cases, a peak in *CO_2 avoided* signifies that reaching higher recovery levels, necessitating increased energy input, may not be the most optimal scenario when the energy source is highly polluting. For the coal at 5 mol% concentration, the values of *CO_2 avoided* are relatively compromised compared to the initial recovery rates, showing a higher production of CO_2 than all the captured CO_2 due to important electricity consumption for recovery higher than 92%.

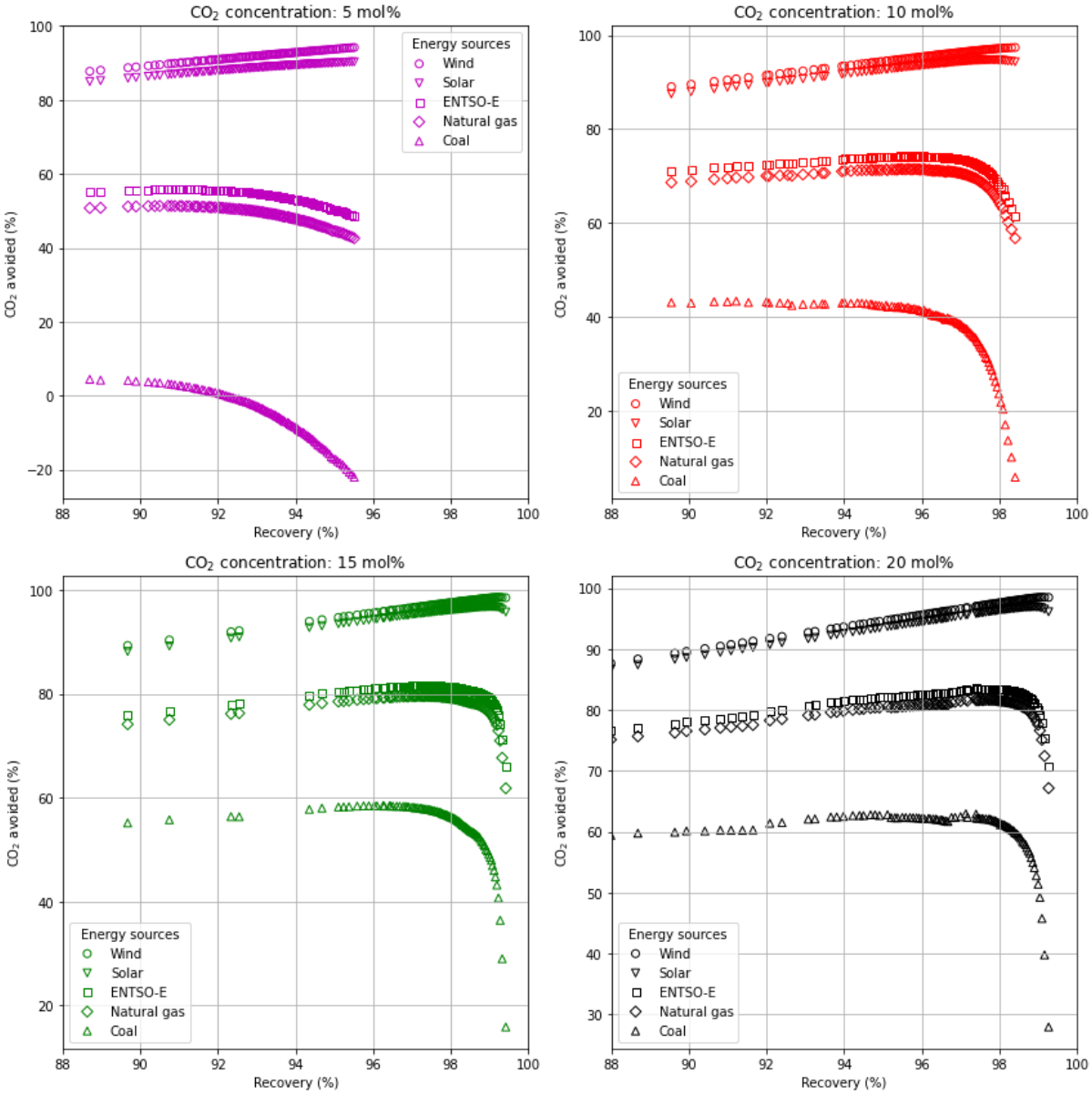

Figure 18: CO_2 avoided as a function of recovery and carbon tax for different inlet CO_2 concentrations. (Emissions factor of electricity ($kg_{CO2e}.kWh^{-1}$): Wind = 0.011; European Network of Transmission System Operators (ENTSO-E) = 0.399; Natural gas = 0.450; Coal = 1.000)

5 Conclusion

The present study investigates the integration of a vacuum pressure swing adsorption process and a carbon purification unit for a hybrid CO_2 capture plant. This approach offers significant advantages, including a high CO_2 recovery facilitated by VPSA and the production of CO_2 with high purity thanks to CPU considering various inlet CO_2 concentrations ranging from 5% to 20%. What makes this process particularly appealing is its reliance on electricity, ensuring a sustainable and environmentally friendly operation and its production of CO_2 matching with all specification needed for CO_2 transportation.

The use of surrogate models for optimization allowed to explore various objectives, such as energy, cost, and CO_2 recovery. The optimization process reveals the intricate interplay between inlet concentrations, recovery rates, and electrical consumption. Notably, the study identifies the trade-off between recovery and electricity consumption, emphasizing the need to balance these factors to achieve an economically viable and environmentally effective carbon capture process. A recovery exceeding 90% can be achieved across different flue gas concentrations. Furthermore, the electrical consumption decreases as the CO_2 content in the feed gas increases, providing a valuable insight into energy efficiency.

The techno-economic analysis emphasizes the significance of minimizing electrical consumption for economic feasibility. The study incorporates considerations of electricity prices and carbon taxes, revealing the effect of these factors on the overall cost structure. The identification of optimal recovery points under different cost scenarios provides crucial information for decision-making and process design.

Taking into consideration the total cost of the process, encompassing CAPEX, OPEX, and the impact of carbon taxes, an inflection point in the recovery levels was identified. This minimum tends towards higher recoveries as carbon taxes rise, underlining the economic and environmental incentives for increased carbon capture.

Additionally, by analyzing the sensitivity of the optimal recovery to variations in electricity prices (ranging from 50 to 200 €.MWh^{-1}), a 10% absolute difference in the optimal recovery value can be achieved. This flexibility is essential for adapting the process to changing economic and regulatory conditions.

One can draw the conclusion that a concentration of 5% is not economically viable, in contrast to other concentrations. For scenarios where the electricity price is below 100 €.MWh^{-1} and the carbon tax exceeds 100 €.t_{CO2}^{-1}, the total capture costs average at 123, 95 and 80 €.t_{CO2}^{-1} for 10%, 15% and 20% CO_2 concentrations in the flue gas, respectively.

This underscores the economic feasibility and attractiveness of the technology for concentrations above 5%, as it aligns with favorable conditions in terms of electricity costs and carbon taxes. Notably, the cost dynamics demonstrate a clear dependency on concentration levels, emphasizing the importance of considering such factors in the strategic planning and decision-making process for implementing carbon capture technologies.

The analysis of the electricity source revealed that the closer one gets to a low-carbon emission energy mix, the more the recovery corresponds to the CO_2 avoided. It is essential, therefore, to consider the nature of electricity production for optimal reduction of carbon emissions; otherwise, a high-recovery operation might be less optimal than lower recoveries.

The sensitivity analysis using Sobol's total order indices sheds light on the key parameters driving recovery and energy consumption. The results underscore the dominant influence of adsorption time, purge time and blowdown pressure, with their importance varying based on CO_2 concentration. This

understanding enables researchers and practitioners to focus on critical parameters for future optimization efforts.

In summary, the research provides a comprehensive understanding of a hybrid CO_2 capture process and offers valuable insights into optimizing it for efficiency, cost-effectiveness, and environmental sustainability. These findings will undoubtedly contribute to the advancement of carbon capture technology and its role in mitigating climate change and reducing greenhouse gas emissions.

CRediT authorship contribution statement

Alexis Costa: Conceptualization, Methodology, Software, Investigation, Data curation, Writing - original draft, Writing - review & editing, Visualization. Arnaud Henrotin: Conceptualization, Methodology, Software, Investigation, Data curation, Writing - original draft, Writing - review & editing, Visualization. Nicolas Heymans: Conceptualization, Methodology, Investigation, Writing - review & editing, Visualization. Lionel Dubois: Writing - review & editing. Diane Thomas: Writing - review & editing. Guy De Weireld: Conceptualization, Validation, Writing - review & editing, Supervision.

Declaration of competing interests

The authors confirm that there are no conflicts to declare.

Acknowledgements

The authors acknowledge the SPF Economie (Belgium) for funding the DRIVER project in the framework of the Energy Transition Fund program.

References

[1] IPCC, SYNTHESIS REPORT OF THE IPCC SIXTH ASSESSMENT REPORT (AR6), Panmao Zhai, 2023.

[2] UNFCCC, The Paris Agreement, (2021). https://unfccc.int/process-and-meetings/the-paris-agreement/the-paris-agreement (accessed October 11, 2021).

[3] A. Runge-Metzger, A Clean Planet for all A European strategic long term vision for a prosperous, modern, competitive and climate neutral economy, 2018.

[4] ZEP, CCS/CCU projects, (2022). https://zeroemissionsplatform.eu/about-ccs-ccu/css-ccu-projects/ (accessed September 15, 2022).

[5] I. Phillips, A. Tucker, P.-O. Granstrom, G. Bozzini, C. Gent, P.J. Capello, A. Clifton, C. Clucas, B. Dolek, P.-Y. Duclos, M. Faou, D. Fletcher, J. Todd, C. Metcalf, F. Neele, M. Reid, J. Senkel, J. Simpson, H. StigterTrevor Crowe, W. Versteele, S. Wong, Network Technology: Guidance for CO_2 transport by ship, 2022.

[6] Fluxys, Carbon Specification Proposal Fluxys Belgium SA, 2022.

[7] E. García-Bordejé, A. Belén Dongil, J.M. Conesa, A. Guerrero-Ruiz, I. Rodríguez-Ramos, Dual functional materials based on Ni and different alkaline metals on alumina for the cyclic stepwise CO_2 capture and methanation, Chemical Engineering Journal 472 (2023). https://doi.org/10.1016/j.cej.2023.144953.

[8] S. Yadav, S.S. Mondal, A review on the progress and prospects of oxy-fuel carbon capture and sequestration (CCS) technology, Fuel 308 (2022). https://doi.org/10.1016/j.fuel.2021.122057.

[9] P. Bains, P. Psarras, J. Wilcox, CO_2 capture from the industry sector, Prog Energy Combust Sci 63 (2017) 146–172. https://doi.org/10.1016/j.pecs.2017.07.001.

[10] C. Chen, S. Yang, The energy demand and environmental impacts of oxy-fuel combustion vs. post-combustion capture in China, Energy Strategy Reviews 38 (2021). https://doi.org/10.1016/j.esr.2021.100701.

[11] N. Bahman, M. Al-Khalifa, S. Al Baharna, Z. Abdulmohsen, E. Khan, Review of carbon capture and storage technologies in selected industries: potentials and challenges, Rev Environ Sci Biotechnol 22 (2023) 451–470. https://doi.org/10.1007/s11157-023-09649-0.

[12] G. Gao, B. Xu, X. Gao, W. Jiang, Z. Zhao, X. Li, C. Luo, F. Wu, L. Zhang, New insights into the structure-activity relationship for CO_2 capture by tertiary amines from the experimental and quantum chemical calculation perspectives, Chemical Engineering Journal 473 (2023) 145277. https://doi.org/10.1016/j.cej.2023.145277.

[13] B. Dziejarski, R. Krzyżyńska, K. Andersson, Current status of carbon capture, utilization, and storage technologies in the global economy: A survey of technical assessment, Fuel 342 (2023). https://doi.org/10.1016/j.fuel.2023.127776.

[14] N.R. Sukor, A.H. Shamsuddin, T.M.I. Mahlia, M.F.M. Isa, Techno-economic analysis of CO_2 capture technologies in offshore natural gas field: Implications to carbon capture and storage in Malaysia, Processes 8 (2020). https://doi.org/10.3390/pr8030350.

[15] A. Gutierrez-Ortega, R. Nomen, J. Sempere, J.B. Parra, M.A. Montes-Morán, R. Gonzalez-Olmos, A fast methodology to rank adsorbents for CO2 capture with temperature swing adsorption, Chemical Engineering Journal 435 (2022). https://doi.org/10.1016/j.cej.2022.134703.

[16] W. Jung, J. Lee, J.S. Lee, New facile process evaluation for membrane-based CO_2 capture: Apparent selectivity model, Chemical Engineering Journal 460 (2023). https://doi.org/10.1016/j.cej.2023.141624.

[17] M.A. Delgado, R. Diego, I. Alvarez, J. Ramos, F. Lockwood, CO_2 balance in a compression and purification unit (CPU), in: Energy Procedia, Elsevier Ltd, 2014: pp. 322–331. https://doi.org/10.1016/j.egypro.2014.11.035.

[18] L. Baxter, C. Hoeger, K. Stitt, S. Burt, A. Baxter, Cryogenic Carbon Capture™ (CCC) Status Report, in: 15th International Conference on Greenhouse Gas Control Technologies, GHGT-15, 2021.

[19] E. Koohestanian, F. Shahraki, Review on principles, recent progress, and future challenges for oxy-fuel combustion CO_2 capture using compression and purification unit, J Environ Chem Eng 9 (2021) 1–20. https://doi.org/10.1016/j.jece.2021.105777.

[20] C. Song, Q. Liu, N. Ji, S. Deng, J. Zhao, Y. Li, Y. Song, H. Li, Alternative pathways for efficient CO_2 capture by hybrid processes—A review, Renewable and Sustainable Energy Reviews 82 (2018) 215–231. https://doi.org/10.1016/j.rser.2017.09.040.

[21] F.B. Torres, J.P. Gutierrez, L.A. Ruiz, M.A. Bertuzzi, E. Erdmann, Comparative analysis of absorption, membrane, and hybrid technologies for CO_2 recovery, J Nat Gas Sci Eng 94 (2021). https://doi.org/10.1016/j.jngse.2021.104082.

[22] R.M. Montañés, L. Riboldi, S. Roussanaly, A. Ouassou, S.G. Subraveti, R. Anantharaman, Techno-economic assessment of the hybrid adsorption-membrane concept for post-combustion CO_2 capture from industry flue gases, (2022). https://ssrn.com/abstract=4282863.

[23] S. Fu, Bench Scale Testing of Next Generation Hollow Fiber Membrane, 2019.

[24] D. Hasse, S. Kulkarni, E. Sanders, E. Corson, J.P. Tranier, CO_2 capture by sub-ambient membrane operation, in: Energy Procedia, Elsevier Ltd, 2013: pp. 993–1003. https://doi.org/10.1016/j.egypro.2013.05.195.

[25] D. Hasse, J. Ma, S. Kulkarni, P. Terrien, J.P. Tranier, E. Sanders, T. Chaubey, J. Brumback, CO_2 capture by cold membrane operation, in: Energy Procedia, Elsevier Ltd, 2014: pp. 186–193. https://doi.org/10.1016/j.egypro.2014.11.019.

[26] T. Chaubey, S. Kulkarni, D. Hasse, A. Augustine, CO_2 Capture by Cold Membrane Operation with Actual Power Plant Flue Gas, 2017.

[27] J.C. Li Yuen Fong, C.J. Anderson, G. Xiao, P.A. Webley, A.F.A. Hoadley, Multi-objective optimisation of a hybrid vacuum swing adsorption and low-temperature post-combustion CO_2 capture, J Clean Prod 111 (2016) 193–203. https://doi.org/10.1016/j.jclepro.2015.08.033.

[28] G. Rodrigues, M. Raventos, R. Dubettier, S. Ruban, Adsorption assisted cryogenic carbon capture: an alternate path to steam driven technologies to decrease cost and carbon footprint, in: 15th International Conference on Greenhouse Gas Control Technologies, 2021. https://ssrn.com/abstract=3820744.

[29] G. Rodrigues, R. Dubettier, M. Tran, B. Cruz, Capturing the benefits of increasing CO_2 concentration in a flue gas through Cryocap™ FG 1, in: 16th International Conference on Greenhouse Gas Control Technologies, 2022. https://ssrn.com/abstract=4284525.

[30] D. Ruthven, Principles of Adsorption and Adsorption Processes, First, John Wiley & Sons, New York, 1984.

[31] C.A. Grande, Advances in Pressure Swing Adsorption for Gas Separation, ISRN Chemical Engineering 2012 (2012) 1–13. https://doi.org/10.5402/2012/982934.

[32] L. Riboldi, O. Bolland, Overview on Pressure Swing Adsorption (PSA) as CO2 Capture Technology: State-of-the-Art, Limits and Potentials, Energy Procedia 114 (2017) 2390–2400. https://doi.org/10.1016/j.egypro.2017.03.1385.

[33] A.K. Rajagopalan, A.M. Avila, A. Rajendran, Do adsorbent screening metrics predict process performance? A process optimisation based study for post-combustion capture of CO2, International Journal of Greenhouse Gas Control 46 (2016) 76–85. https://doi.org/10.1016/j.ijggc.2015.12.033.

[34] K.T. Chue, J.N. Kim, Y.J. Yoo, S.H. Cho, R.T. Yang, Comparison of Activated Carbon and Zeolite 13X for CO2 Recovery from Flue Gas by Pressure Swing Adsorption, Ind Eng Chem Res 34 (1995) 591–598. https://doi.org/10.1021/ie00041a020.

[35] Z. Hu, Y. Wang, B.B. Shah, D. Zhao, CO 2 Capture in Metal–Organic Framework Adsorbents: An Engineering Perspective, Adv Sustain Syst 3 (2019) 1800080. https://doi.org/10.1002/adsu.201800080.

[36] F. Raganati, F. Miccio, P. Ammendola, Adsorption of Carbon Dioxide for Post-combustion Capture: A Review, Energy & Fuels 35 (2021) 12845–12868. https://doi.org/10.1021/acs.energyfuels.1c01618.

[37] G. Li, P. Xiao, P. Webley, J. Zhang, R. Singh, M. Marshall, Capture of CO2 from high humidity flue gas by vacuum swing adsorption with zeolite 13X, Adsorption 14 (2008) 415–422. https://doi.org/10.1007/s10450-007-9100-y.

[38] C.W. Skarstrom, Method and apparatus for fractionating gaseous mixtures by adsorption, US2944627, 1960.

[39] C. Shen, J. Yu, P. Li, C.A. Grande, A.E. Rodrigues, Capture of CO2 from flue gas by vacuum pressure swing adsorption using activated carbon beads, Adsorption 17 (2011) 179–188. https://doi.org/10.1007/s10450-010-9298-y.

[40] N. Jiang, Y. Shen, B. Liu, D. Zhang, Z. Tang, G. Li, B. Fu, CO2 capture from dry flue gas by means of VPSA, TSA and TVSA, Journal of CO2 Utilization 35 (2020) 153–168. https://doi.org/10.1016/j.jcou.2019.09.012.

[41] Z. Liu, C.A. Grande, P. Li, J. Yu, A.E. Rodrigues, Multi-bed vacuum pressure swing adsorption for carbon dioxide capture from flue gas, Sep Purif Technol 81 (2011) 307–317. https://doi.org/10.1016/j.seppur.2011.07.037.

[42] R. Haghpanah, A. Majumder, R. Nilam, A. Rajendran, S. Farooq, I.A. Karimi, M. Amanullah, Multiobjective optimization of a four-step adsorption process for postcombustion CO2 capture via finite volume simulation, Ind Eng Chem Res 52 (2013) 4249–4265. https://doi.org/10.1021/ie302658y.

[43] R. Haghpanah, R. Nilam, A. Rajendran, S. Farooq, I.A. Karimi, Cycle synthesis and optimization of a VSA process for postcombustion CO 2 capture, AIChE Journal 59 (2013) 4735–4748. https://doi.org/10.1002/aic.14192.

[44] S. Krishnamurthy, V.R. Rao, S. Guntuka, P. Sharratt, R. Haghpanah, A. Rajendran, M. Amanullah, I.A. Karimi, S. Farooq, CO 2 capture from dry flue gas by vacuum swing adsorption: A pilot plant study, AIChE Journal 60 (2014) 1830–1842. https://doi.org/10.1002/aic.14435.

[45] L. Wang, Z. Liu, P. Li, J. Wang, J. Yu, CO2 capture from flue gas by two successive VPSA units using 13XAPG, Adsorption 18 (2012) 445–459. https://doi.org/10.1007/s10450-012-9431-1.

[46] J. Zhang, P.A. Webley, P. Xiao, Effect of process parameters on power requirements of vacuum swing adsorption technology for CO2 capture from flue gas, Energy Convers Manag 49 (2008) 346–356. https://doi.org/10.1016/j.enconman.2007.06.007.

[47] P. Xiao, J. Zhang, P. Webley, G. Li, R. Singh, R. Todd, Capture of CO2 from flue gas streams with zeolite 13X by vacuum-pressure swing adsorption, Adsorption 14 (2008) 575–582. https://doi.org/10.1007/s10450-008-9128-7.

[48] C. Kolster, E. Mechleri, S. Krevor, N. Mac Dowell, The role of CO_2 purification and transport networks in carbon capture and storage cost reduction, International Journal of Greenhouse Gas Control 58 (2017) 127–141. https://doi.org/10.1016/j.ijggc.2017.01.014.

[49] B. Jin, H. Zhao, C. Zheng, Thermoeconomic cost analysis of CO_2 compression and purification unit in oxy-combustion power plants, Energy Convers Manag 106 (2015) 53–60. https://doi.org/10.1016/j.enconman.2015.09.014.

[50] B. Jin, H. Zhao, C. Zheng, Optimization and control for CO_2 compression and purification unit in oxy-combustion power plants, Energy 83 (2015) 416–430. https://doi.org/10.1016/j.energy.2015.02.039.

[51] H. Li, Y. Hu, M. Ditaranto, D. Willson, J. Yan, Optimization of cryogenic CO_2 purification for oxy-coal combustion, Energy Procedia 37 (2013) 1341–1347. https://doi.org/10.1016/j.egypro.2013.06.009.

[52] F. Magli, M. Spinelli, M. Fantini, M.C. Romano, M. Gatti, Techno-economic optimization and off-design analysis of CO_2 purification units for cement plants with oxyfuel-based CO_2 capture,

International Journal of Greenhouse Gas Control 115 (2022) 103591. https://doi.org/10.1016/j.ijggc.2022.103591.

[53] W.L. Luyben, Simple control structure for a compression purification process in an oxy-combustion power plant, AIChE Journal 61 (2015) 1581–1588. https://doi.org/10.1002/aic.14754.

[54] E. Koohestanian, J. Sadeghi, D. Mohebbi Kalhori, F. Shahraki, A. Samimi, New Process Flowsheet for CO_2 Compression and Purification Unit; Dynamic Investigation and Control, J. Chem. Chem. Eng. Research Article 40 (2021) 593–604. https://doi.org/https://doi.org/10.30492/ijcce.2020.37779.

[55] M.M. Shah, Carbon dioxide (CO_2) compression and purification technology for oxy-fuel combustion, in: Oxy-Fuel Combustion for Power Generation and Carbon Dioxide (CO_2) Capture, Woodhead Publishing Limited, 2011: pp. 228–255. https://doi.org/10.1533/9780857090980.2.228.

[56] N. Chambron, P. Terrien, Capture de CO_2 par unité cryogénique sur une centrale de type gazéification intégrée à cycle combiné, FR2997866A3, 2014.

[57] Q. Zhang, Y. Li, Q. Zhang, F. Ma, X. Lü, Application of deep dehumidification technology in low-humidity industry: A review, Renewable and Sustainable Energy Reviews 193 (2024) 114278. https://doi.org/10.1016/j.rser.2024.114278.

[58] Y. Yang, Y. Chen, Z. Xu, L. Wang, P. Zhang, A three-bed six-step TSA cycle with heat carrier gas recycling and its model-based performance assessment for gas drying, Sep Purif Technol 237 (2020) 116335. https://doi.org/10.1016/J.SEPPUR.2019.116335.

[59] J. Zhang, P.A. Webley, Cycle development and design for CO2 capture from flue gas by vacuum swing adsorption, Environ Sci Technol 42 (2008) 563–569. https://doi.org/10.1021/es0706854.

[60] L. Wang, Y. Yang, W. Shen, X. Kong, P. Li, J. Yu, A.E. Rodrigues, Experimental evaluation of adsorption technology for CO2 capture from flue gas in an existing coal-fired power plant, Chem Eng Sci 101 (2013) 615–619. https://doi.org/10.1016/j.ces.2013.07.028.

[61] X. Yu, B. Liu, Y. Shen, D. Zhang, Design and experiment of high-productivity two-stage vacuum pressure swing adsorption process for carbon capturing from dry flue gas, Chin J Chem Eng 43 (2022) 378–391. https://doi.org/10.1016/j.cjche.2021.02.022.

[62] A.H. Farmahini, S. Krishnamurthy, D. Friedrich, S. Brandani, L. Sarkisov, From Crystal to Adsorption Column: Challenges in Multiscale Computational Screening of Materials for Adsorption Separation Processes, Ind Eng Chem Res 57 (2018) 15491–15511. https://doi.org/10.1021/acs.iecr.8b03065.

[63] X. Hu, E. Mangano, D. Friedrich, H. Ahn, S. Brandani, Diffusion mechanism of CO2 in 13X zeolite beads, Adsorption 20 (2014) 121–135. https://doi.org/10.1007/s10450-013-9554-z.

[64] A.G. Dixon, Correlations for wall and particle shape effects on fixed bed bulk voidage, Can J Chem Eng 66 (1988) 705–708. https://doi.org/10.1002/cjce.5450660501.

[65] A.S. Pushnov, Calculation of average bed porosity, Chemical and Petroleum Engineering 42 (2006) 14–17. https://doi.org/10.1007/s10556-006-0045-x.

[66] J.A.A. Gibson, E. Mangano, E. Shiko, A.G. Greenaway, A. V. Gromov, M.M. Lozinska, D. Friedrich, E.E.B. Campbell, P.A. Wright, S. Brandani, Adsorption Materials and Processes for Carbon Capture from Gas-Fired Power Plants: AMPGas, Ind Eng Chem Res 55 (2016) 3840–3851. https://doi.org/10.1021/acs.iecr.5b05015.

[67] P.A. Webley, A. Qader, A. Ntiamoah, J. Ling, P. Xiao, Y. Zhai, A New Multi-bed Vacuum Swing Adsorption Cycle for CO2 Capture from Flue Gas Streams, Energy Procedia 114 (2017) 2467–2480. https://doi.org/10.1016/j.egypro.2017.03.1398.

[68] L. Jiang, V.G. Fox, L.T. Biegler, Simulation and optimal design of multiple-bed pressure swing adsorption systems, AIChE Journal 50 (2004) 2904–2917. https://doi.org/10.1002/aic.10223.

[69] G. Langer, A. Roethe, K.P. Roethe, D. Gelbin, Heat and mass transfer in packed beds-III. Axial mass dispersion, Int J Heat Mass Transf 21 (1978) 751–759. https://doi.org/10.1016/0017-9310(78)90037-6.

[70] S. Sircar, J.R. Hufton, Why does the linear driving force model for adsorption kinetics work?, Adsorption 6 (2000) 137–147. https://doi.org/10.1023/A:1008965317983.

[71] RalphT. Yang, Gas Separation by Adsorption Processes, Elsevier, 1987. https://doi.org/10.1016/C2013-0-04269-7.

[72] M. Kaviany, A. Kanury, Principles of Heat Transfer, Appl Mech Rev 55 (2002) B100–B102. https://doi.org/10.1115/1.1497490.

[73] J. Beek, Design of Packed Catalytic Reactors, Advances in Chemical Engineering 3 (1962) 203–271. https://doi.org/10.1016/S0065-2377(08)60060-5.

[74] F.P. Incropera, D.P. DeWitt, Fundamentals of Heat and Mass Transfer, (1996) 890. https://doi.org/10.1016/j.applthermaleng.2011.03.022.

[75] M.S. Shafeeyan, W.M.A. Wan Daud, A. Shamiri, A review of mathematical modeling of fixed-bed columns for carbon dioxide adsorption, Chemical Engineering Research and Design 92 (2014) 961–988. https://doi.org/10.1016/j.cherd.2013.08.018.

[76] G. Soave, Equilibrium constants from a modified Redlich-Kwong equation of state, Chem Eng Sci 27 (1972) 1197–1203. https://doi.org/10.1016/0009-2509(72)80096-4.

[77] R.S. Brokaw, Approximate Formulas for the Viscosity and Thermal Conductivity of Gas Mixtures. II, J Chem Phys 42 (1965) 1140–1146. https://doi.org/10.1063/1.1696093.

[78] C.R. Wilke, A Viscosity Equation for Gas Mixtures, J Chem Phys 18 (1950) 517–519. https://doi.org/10.1063/1.1747673.

[79] E.A. Mason, S.C. Saxena, Approximate Formula for the Thermal Conductivity of Gas Mixtures, Phys Fluids 1 (1958) 361–369. https://doi.org/10.1063/1.1724352.

[80] B.E. Poling, J.M. Prausnitz, J.P. O'Connell, The properties of gases and liquids, Fifth Edit, McGraw-Hill, 2001. https://pubs.aip.org/physicstoday/article/12/4/38/895367/The-Properties-of-Gases-and-Liquids.

[81] G. Béasse, C. Bourhy-Weber, S. Daeden, L. Granados, F. Lockwood, P. Moreschini, M. Rivière, Callide Oxyfuel Project Callide Oxyfuel Project Results from the CPU, Ponferrada, 2013.

[82] T. Lockwood, Developments in oxyfuel combustion of coal, IEA Clean Coal Centre, 2014.

[83] A. Costa, D. Coppitters, L. Dubois, F. Contino, D. Thomas, G. De Weireld, Energy, exergy, economic and environmental (4E) analysis of a cryogenic carbon purification unit with membrane for oxyfuel cement plant flue gas, Appl Energy 357 (2024) 122431. https://doi.org/10.1016/j.apenergy.2023.122431.

[84] D.-Y. Peng, D.B. Robinson, A New Two-Constant Equation of State, Industrial & Engineering Chemistry Fundamentals 15 (1976) 59–64. https://doi.org/10.1021/i160057a011.

[85] S. Lasala, P. Chiesa, R. Privat, J.N. Jaubert, VLE properties of CO_2 – Based binary systems containing N_2, O_2 and Ar: Experimental measurements and modelling results with advanced cubic equations of state, Fluid Phase Equilib 428 (2016) 18–31. https://doi.org/10.1016/J.FLUID.2016.05.015.

[86] M.W. Stanley, Selection and Design, Butterwoths Series in Chemical Engineering, Chemical Process Equipment, 1990.

[87] Y. Xin, Y. Zhang, P. Xue, K. Wang, E. Adu, P. Tontiwachwuthikul, The optimization and thermodynamic and economic estimation analysis for CO_2 compression-liquefaction process of CCUS system using LNG cold energy, Energy 236 (2021) 121376. https://doi.org/10.1016/j.energy.2021.121376.

[88] R.T. Maruyama, K.N. Pai, S.G. Subraveti, A. Rajendran, Improving the performance of vacuum swing adsorption based CO_2 capture under reduced recovery requirements, International Journal of Greenhouse Gas Control 93 (2020). https://doi.org/10.1016/j.ijggc.2019.102902.

[89] R. Turton, J.A. Shaeiwitz, D. Bhattacharyya, W.B. Whiting, Analysis, Synthesis, and Design of Chemical Processes, Pearson Education, Inc, 2018.

[90] C. Maxwell, Cost Indices, (2022). https://www.toweringskills.com/financial-analysis/cost-indices/ (accessed August 30, 2022).

[91] Linde, Aluminium plate-fin heat exchangers, n.d.

[92] S.G. Subraveti, S. Roussanaly, R. Anantharaman, L. Riboldi, A. Rajendran, Techno-economic assessment of optimised vacuum swing adsorption for post-combustion CO_2 capture from steam-methane reformer flue gas, Sep Purif Technol 256 (2021). https://doi.org/10.1016/j.seppur.2020.117832.

[93] R. Chauvy, L. Dubois, P. Lybaert, D. Thomas, G. De Weireld, Production of synthetic natural gas from industrial carbon dioxide, Appl Energy 260 (2020) 114249. https://doi.org/10.1016/J.APENERGY.2019.114249.

[94] Y. Da Hsiao, C.T. Chang, Progressive learning for surrogate modeling of amine scrubbing CO_2 capture processes, Chemical Engineering Research and Design 194 (2023) 653–665. https://doi.org/10.1016/j.cherd.2023.05.016.

[95] J. Beck, D. Friedrich, S. Brandani, E.S. Fraga, Multi-objective optimisation using surrogate models for the design of VPSA systems, Comput Chem Eng 82 (2015) 318–329. https://doi.org/10.1016/j.compchemeng.2015.07.009.

[96] W. Chung, J. Kim, J.H. Lee, First-principles based surrogate modeling of pressure swing adsorption processes for CO_2 capture, in: IFAC-PapersOnLine, Elsevier B.V., 2022: pp. 310–315. https://doi.org/10.1016/j.ifacol.2022.07.462.

[97] A.I.J. Forrester, A. Sóbester, A.J. Keane, Engineering Design via Surrogate Modelling, Wiley, 2008. https://doi.org/10.1002/9780470770801.

[98] J. Kudela, R. Matousek, Recent advances and applications of surrogate models for finite element method computations: a review, Soft Comput 26 (2022) 13709–13733. https://doi.org/10.1007/s00500-022-07362-8.

[99] Constructing a Surrogate, in: Engineering Design via Surrogate Modelling, John Wiley & Sons, Ltd, Chichester, UK, 2008: pp. 33–76. https://doi.org/10.1002/9780470770801.ch2.

[100] J. Sacks, S.B. Schiller, W.J. Welch, Designs for Computer Experiments, Technometrics 31 (1989) 41. https://doi.org/10.2307/1270363.

[101] R. Jin, W. Chen, A. Sudjianto, An efficient algorithm for constructing optimal design of computer experiments, J Stat Plan Inference 134 (2005) 268–287. https://doi.org/10.1016/j.jspi.2004.02.014.

[102] P. Saves, R. Lafage, N. Bartoli, Y. Diouane, J. Bussemaker, T. Lefebvre, J.T. Hwang, J. Morlier, J.R.R.A. Martins, SMT 2.0: A Surrogate Modeling Toolbox with a focus on Hierarchical and Mixed Variables Gaussian Processes, (2023) 1–37. http://arxiv.org/abs/2305.13998.

[103] J. Beck, D. Friedrich, S. Brandani, E.S. Fraga, Multi-objective optimisation using surrogate models for the design of VPSA systems, Comput Chem Eng 82 (2015) 318–329. https://doi.org/10.1016/j.compchemeng.2015.07.009.

[104] E.T. Spiller, M.J. Bayarri, J.O. Berger, E.S. Calder, A.K. Patra, E.B. Pitman, R.L. Wolpert, Automating Emulator Construction for Geophysical Hazard Maps, SIAM/ASA Journal on Uncertainty Quantification 2 (2014) 126–152. https://doi.org/10.1137/120899285.

[105] I.M. Sobol, Global sensitivity indices for nonlinear mathematical models and their Monte Carlo estimates, 55 (2001) 271–280.

[106] T. Iwanaga, W. Usher, J. Herman, Toward SALib 2.0: Advancing the accessibility and interpretability of global sensitivity analyses, Socio-Environmental Systems Modelling 4 (2022) 18155. https://doi.org/10.18174/sesmo.18155.

[107] S. Kucherenko, O. V. Klymenko, N. Shah, Sobol' indices for problems defined in non-rectangular domains, Reliab Eng Syst Saf 167 (2017) 218–231. https://doi.org/10.1016/j.ress.2017.06.001.

[108] H. Seada, K. Deb, A Unified Evolutionary Optimization Procedure for Single, Multiple, and Many Objectives, IEEE Transactions on Evolutionary Computation 20 (2016) 358–369. https://doi.org/10.1109/TEVC.2015.2459718.

[109] J. Blank, K. Deb, Pymoo: Multi-Objective Optimization in Python, IEEE Access 8 (2020) 89497–89509. https://doi.org/10.1109/ACCESS.2020.2990567.

[110] EMBER, Carbon Price Tracker, (2023). https://ember-climate.org/data/data-tools/carbon-price-viewer/ (accessed March 13, 2023).